

DTIC FILE COPY

**The Influence of Surface Roughness and
Bubbles on Sea Surface Acoustic Backscattering**

***Der Einfluss von Seegangsrauhigkeit und
Blasen auf die akustischen Rückstreuungseigen-
schaften der Meeresoberfläche***

**Bernd Nützel
Heinz Herwig**

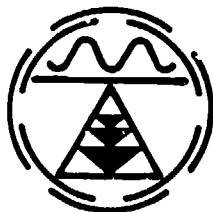
*Forschungsanstalt der Bundeswehr
für Wasserschall- und Geophysik*

**Joseph M. Monti
Paul D. Koenigs**

*Surface Ship Sonar Department
Naval Underwater Systems Center*

12 November 1987

DTIC
ELECTE
FEB 01 1988
S D



**FORSCHUNGSANSTALT DER BUNDESWEHR
FÜR WASSERSCHALL- UND GEOPHYSIK
Kiel**



**NAVAL UNDERWATER SYSTEMS CENTER
Newport, Rhode Island • New London, Connecticut**

Approved for public release; distribution is unlimited.

58 1 25 095

AD-A191 298

Vorwort

Die Messungen an der Forschungsplattform NORDSEE wurden im Rahmen des Datenaustauschabkommens MWDDEA-N-67-G-4207, Subproject 2, durchgeführt. Die Abstimmung des jährlichen Forschungsprogrammes der FWG mit dem Inhalt des DEA erfolgte durch RüFo 3 des BMVg der Bundesrepublik Deutschland.

Preface

This document describes work performed under Data Exchange Agreement MWDDEA-N-67-G-4207, Subproject 2, between the Forschungsanstalt der Bundeswehr fuer Wasserschall- und Geophysik (FWG), Kiel, Federal Republic of Germany (FRG), and the Naval Underwater Systems Center (NUSC), New London, Connecticut, USA. The U.S. effort was accomplished under NUSC Project No. B68201, "Environmental Dependence of Acoustic Surface Scatter," Principal Investigator P. D. Koenigs (NUSC Code 3321). Funding was provided under Program Element 62759N by Naval Sea Systems Command (NAVSEA 63R), Dr. R. Farwell (NORDA 113), Manager. The work was performed under the auspices of the Office of Naval Research (Code 102D).

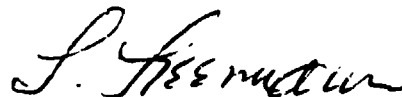
The Technical Reviewer for this report was P. D. Herstein (NUSC Code 33A3).

EINVERSTANDEN: 11 September 1987



PROF. Dr. G. Ziehm
Director, Defence Research Institute
for Underwater Sound and Geophysics
Federal Republic of Germany

APPROVED: 12 November 1987



L. Freeman
Surface Ship Sonar Department
Naval Underwater Systems Center

The Influence of Surface Roughness and Bubbles on Sea Surface Acoustic Backscattering

Der Einfluss von Seegangsrauhigkeit und Blasen auf die akustischen Rückstreuungseigenschaften der Meeresoberfläche

**Bernd Nützel
Heinz Herwig**

*Forschungsanstalt der Bundeswehr
für Wasserschall- und Geophysik*

**Joseph M. Monti
Paul D. Koenigs**

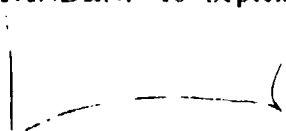
*Surface Ship Sonar Department
Naval Underwater Systems Center*

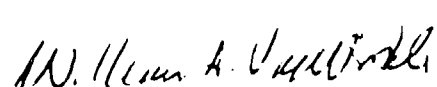
This report is the result of a cooperative research project conducted under the auspices of ONR's data exchange agreement MWDDEA-N-67-G-4207, Subproject 2.



EINVERSTANDEN: 16 September 1987

APPROVED: 30 November 1987


Min Rat Dreher
German Project Officer
MOD Bonn, Code Rü V4


Dr. William A. Von Winkle
Naval Underwater Systems Center
for the United States Project Officer

on For	
RA&I	<input checked="" type="checkbox"/>
U	<input type="checkbox"/>
and	<input type="checkbox"/>
ation	
ation/	
bility Codes	
ail and/or	
Special	

P-1

UNCLASSIFIED

SECURITY CLASSIFICATION OF THIS PAGE

REPORT DOCUMENTATION PAGE

1a. REPORT SECURITY CLASSIFICATION UNCLASSIFIED			1b. RESTRICTIVE MARKINGS		
2a. SECURITY CLASSIFICATION AUTHORITY			3. DISTRIBUTION/AVAILABILITY OF REPORT Approved for public release; distribution is unlimited.		
2b. DECLASSIFICATION/DOWNGRADING SCHEDULE			5. MONITORING ORGANIZATION REPORT NUMBER(S)		
4. PERFORMING ORGANIZATION REPORT NUMBER(S) NUSC TR 7955					
6a. NAME OF PERFORMING ORGANIZATION Naval Underwater Systems Center		6b. OFFICE SYMBOL (If applicable) 3331		7a. NAME OF MONITORING ORGANIZATION	
6c. ADDRESS (City, State, and ZIP Code) New London Laboratory New London, CT 06320		7b. ADDRESS (City, State, and ZIP Code)			
8a. NAME OF FUNDING/SPONSORING ORGANIZATION Office of Naval Research		8b. OFFICE SYMBOL (If applicable) 102D		9. PROCUREMENT INSTRUMENT IDENTIFICATION NUMBER	
8c. ADDRESS (City, State, and ZIP Code) Arlington, VA 22217		10. SOURCE OF FUNDING NUMBERS			
		PROGRAM ELEMENT NO. 62759N	PROJECT NO. B68201	TASK NO.	WORK UNIT ACCESSION NO. TD0832
11. TITLE (Include Security Classification) THE INFLUENCE OF SURFACE ROUGHNESS AND BUBBLES ON SEA SURFACE ACOUSTIC BACKSCATTERING					
12. PERSONAL AUTHOR(S) B. Nützel and H. Herwig (FWG); J. Monti and P. Koenigs (NUSC)					
13a. TYPE OF REPORT FINAL		13b. TIME COVERED FROM 10/85 TO 9/86		14. DATE OF REPORT (Year, Month, Day) 12 November 1987	
15. PAGE COUNT 56					
16. SUPPLEMENTARY NOTATION					
17. COSATI CODES			18. SUBJECT TERMS (Continue on reverse if necessary and identify by block number)		
FIELD	GROUP	SUB-GROUP	→ Acoustic Scattering Strength, Frequency Dependence		
08	03		Backward Surface Scatter, Grazing Angle Dependence		
20	01		Bubbles, High Resolution ←		
19. ABSTRACT (Continue on reverse if necessary and identify by block number)					
<p>Im Rahmen eines Datenaustauschabkommens zwischen den Vereinigten Staaten und der Bundesrepublik Deutschland wurden im Herbst 1985 an der Forschungsplattform "NORDSEE" Untersuchungen zu den akustischen Streueigenschaften der Meeresoberfläche durchgeführt. Die Ergebnisse dieses Experimentes werden gemeinsam mit den Seegangsparemtern dargelegt.</p>			<p>The results from a recent sea surface acoustic scattering experiment, which was conducted in the North Sea, are presented with accompanying sea surface roughness parameters and subsurface bubble information. The acoustic data were obtained utilizing a high-resolution (narrow beamwidth) pulsed parametric sonar transmitter and conventional receiver. Scattering strength values were obtained as a function of frequency (3-18 kHz) and grazing angle (15 to 90°) for differing sea surface roughness and wind speed conditions.</p>		
20. DISTRIBUTION/AVAILABILITY OF ABSTRACT <input checked="" type="checkbox"/> UNCLASSIFIED/UNLIMITED <input type="checkbox"/> SAME AS RPT. <input type="checkbox"/> DTIC USERS			21. ABSTRACT SECURITY CLASSIFICATION UNCLASSIFIED		
22a. NAME OF RESPONSIBLE INDIVIDUAL Joseph M. Monti			22b. TELEPHONE (Include Area Code) (203) 440-5849		22c. OFFICE SYMBOL 3112

18. (Cont'd.)

NORDSEE Research Platform

→ North Sea
Parametric Sonar
Radar Backscatter

Roughness Dependence
Shallow Water
Waveheight Dependence
Wind Dependence

18

19. (Cont'd.)

Als Schallquelle diente ein parametrischer Wandler hoher Richtwirkung, der im konventionellen Betrieb als Empfänger arbeitete. Rückstreustärken wurden in Abhängigkeit der Frequenz (3 bis 18 kHz) und des Glanzwinkels (15 bis 90°) für verschiedene Windgeschwindigkeiten und Seezustände gewonnen.

Die bestimmenden Rückstreumechanismen sind Blasen bei hohen Windgeschwindigkeiten und flachen Glanzwinkeln und das hochfrequente Seejangsspektrum bei allen Glanzwinkeln. Bei mittleren Windgeschwindigkeiten weist die Rückstreustärke starke zeitliche Fluktuationen auf, die von beiden Streumechanismen verursacht werden.

The dominant backscattering mechanisms are bubbles at high wind speeds and low grazing angles and the high frequency ocean wavenumber spectrum at low wind speeds and all grazing angles. In an intermediate wind speed regime, the time history of backscattering shows strong fluctuations, which are caused by both scattering mechanisms.

Keywords:

TABLE OF CONTENTS

	Page
LIST OF ILLUSTRATIONS	ii
LIST OF TABLES.	iii
1.0 INTRODUCTION	1
2.0 EXPERIMENTAL SETUP	1
2.1 Geographic Location.	1
2.2 Sensor Locations	2
2.3 Acoustic Sensor.	3
2.4 Data Acquisition and Processing.	4
3.0 SUPPORTING MEASUREMENTS.	13
3.1 Meteorological	13
3.1.1 Precipitation	13
3.1.2 Wind Velocity.	13
3.2 Oceanographic.	13
3.2.1 Tides.	13
3.2.2 Sound Speed.	14
3.2.3 Sea Surface Characteristics.	14
3.2.3.1 Wave Rider Buoy.	14
3.2.3.2 Stilwell Photography	15
3.2.3.3 VCR.	15
3.3 Bubble Measurements.	16
3.4 Electromagnetic (Radar) Measurements	16
4.0 ACOUSTIC SURFACE AND SUBSURFACE SCATTERING	19
4.1 Theory	19
4.1.1 Background	19
4.1.2 Incoherent Scattering.	19
4.1.3 Coherent Scattering.	22
4.2 Measurement.	23
4.2.1 Data Set	23
4.2.2 Data Analysis.	23
4.3 Backscatter Results.	25
4.3.1 Saturation	25
4.3.2 Grazing Angle Dependence	26
4.3.3 Frequency Dependence	27
4.3.4 Specular Point	27
4.3.5 Temporal Variability	27
4.4 Comparison With Theory and Other Measurements.	31
5.0 CONCLUSIONS.	46
6.0 RECOMMENDATIONS	48
7.0 REFERENCES	50

LIST OF ILLUSTRATIONS

Figure		Page
2-1	Measurement Location	6
2-2	FPN Schematic -- Side View	7
2-3	FPN Schematic -- Top View	8
2-4	Acoustic Sensor and Mounting Tower	9
2-5	Transmit Voltage Response of Acoustic Source	10
2-6	Insonification Area	10
2-7	Receiving Beampatterns of Acoustic Sensor in Conventional Receive Mode	11
2-8	Flow Diagram for the Transmit Signal Generation	12
2-9	Flow Diagram for the Receiving Signal Data Acquisition	12
3-1	Influence of Wind Velocity on Water Height	17
3-2	Sound Speed Profile on 14 November 1986	17
3-3	Significant Waveheight vs. Wind Speed During NOREX-85	18
3-4	Directional Spectrum of the Sea Surface Using Stilwell's Technique	18
4-1	Principal Features Affecting Acoustic Surface Scattering	33
4-2	Scattering Cross Section of Air Bubbles at 10 kHz	33
4-3	Sea Surface Backscatter vs. Grazing Angle (Saturation).	34
4-4	Backscatter vs. Wind Speed for a 30-deg Grazing Angle (Frequency Dependence of Saturation Onset)	34
4-5	Backscatter vs. Wind Speed for a 15-deg Grazing Angle (Frequency Dependence of Saturation Onset)	35
4-6	Backscattering Strength vs. Grazing Angle for Different Frequencies	35
4-7	Backscattering Strength vs. Grazing Angle at 10 kHz for Different Wind Speeds	36
4-8	Backscattering Strength at 3 kHz With and Without Sea Surface Ripples	36
4-9	Frequency Dependence of Backscatter at Various Grazing Angles	37
4-10	Normal Incidence Backscatter vs. Wind Speed	37
4-11	Normal Incidence Backscatter Illustrating the Effect of Rainfall	38
4-12	Single Ping Acoustic Reverberation at Normal Incidence.	38
4-13	Reverberation Level vs. Time From Surface and Bubble Scatterers at Normal Incidence	39
4-14	Ensemble-Averaged Acoustic Reverberation at Normal Incidence.	39
4-15	Variability of Backscattering Strength at 3 kHz	40
4-16	Time History of Backscatter Energy	41
4-17	Coefficient of Variation for Three Frequencies as a Function of Wind Speed for a 30-deg Grazing Angle.	41
4-18	Time History of Backscatter Energy for Different Wind Speeds	42
4-19	Scattering Mechanism Contribution as a Function of Wind Speed and Frequency at a 30-deg Grazing Angle.	43
4-20	Temporal Variability of Backscatter at 10 kHz for a 30-deg Grazing Angle at Three Wind Speeds	43

LIST OF ILLUSTRATIONS (Cont'd)

Figure		Page
4-21	Comparison of Chapman-Harris and Eckart Semiempirical Model With NOREX-85 Data	44
4-22	Comparison of McCammon and McDaniel Theoretical Model With NOREX-85 Data	44
4-23	Comparison of McDaniel and Gorman Theoretical Model and Measured Data With NOREX-85 Data	45

LIST OF TABLES

Table		Page
2-1	Model Results of Source Level and Beamwidth for NOREX-85 Data	3
4-1	NOREX-85 Data Set	24

THE INFLUENCE OF SURFACE ROUGHNESS AND BUBBLES ON SEA SURFACE ACOUSTIC BACKSCATTERING

1.0 INTRODUCTION

In the fall of 1985, a cooperative experiment was conducted for a 5-week period in the shallow water area of the North Sea known as the German Bight. Participants in the experiment were the Forschungsanstalt der Bundeswehr fuer Wasserschall-und -physik (FWG), Kiel, Federal Republic of Germany; the Naval Underwater Systems Center (NUSC), New London, Connecticut; and the Naval Oceanographic Research and Development Activity (NORDA), Bay St. Louis, Mississippi.

The objectives of the experiment were (1) to determine the dependence of acoustic scattering from the sea surface on environmental conditions at audio frequencies and (2) to investigate the regimes over which large-scale sea surface roughness, small-scale roughness, and subsurface bubble population are the predominant scattering mechanisms.

The acoustic measurements were made with a parametric source and a conventional receiver in the frequency range of 3 to 18 kHz. Acoustic sea surface backscatter data were obtained from normal incidence (90 deg) to grazing angles of 15 deg. During the data collection periods, wind speeds ranged from 1 to 19 knots and significant waveheights varied from 0.4 to 4.5 m. Thus, a unique acoustic data set was obtained. This set was supported with a broad range of environmental measurements, such as wind velocity, precipitation, significant waveheight, sound speed profiles, subsurface bubble densities, radar backscatter, and sea surface directional and nondirectional spectra.

This report describes the data acquisition and analysis techniques, sea surface backscatter results, and the correlation of these results with environmental parameters.

2.0 EXPERIMENTAL SETUP

2.1 GEOGRAPHIC LOCATION

The experiment site was the Federal Republic of Germany's research platform NORDSEE (Forschungsplattform NORDSEE(FPN)), which is approximately 40 nautical miles west of the West German and Danish coasts at 54°42' N - 7°10' E (see figure 2-1).

In most cases the fall weather in the German Bight is driven by rapidly moving low pressure systems coming from the Atlantic. Therefore, the sea state is normally duration and not fetch limited because the wind velocity

decorrelation time in the North Sea is only a few hours. In the vicinity of the platform there are tidal currents of up to 2 knots in northwesterly and southeasterly directions. From October to April the water temperature is constant in depth; hence, a nearly isovelocity condition exists in the winter and straight line acoustic propagation can be assumed.

2.2 SENSOR LOCATIONS

The research platform is located in approximately 30 m of water and is fixed to the sea floor. It is equipped to make standard oceanographic measurements of wind velocity, waveheight, tide, and temperature.

Other measurements in support of the underwater acoustic experiment were also made. These measurements consisted of sound speed profiles, wave characteristics, subsurface bubbles, and electromagnetic scattering (radar). The location of these measuring devices can be seen in figure 2-2.

Ocean wave characteristics were obtained with several different apparatus. A wave rider buoy, located approximately 500 m west of the platform, was utilized to obtain real-time significant waveheight ($H_{1/3}$) and ocean wave nondirectional spectra from 0 to 0.3 Hz. A wave array was suspended from crane A (figure 2-3), which consisted of seven wave sensors in a hexagonal arrangement with a nominal spacing of about 1 m. Each wave sensor had a frequency response from 0 to 1.5 Hz, and the entire wave array was capable of providing directional wave spectra from 0 to 0.5 Hz.

High frequency directional wave measurements in the range of approximately 1.5 to 4 Hz were made using photographs of the sea surface and Stilwell's processing technique as modified by Baur.¹ In addition to quantitative measurements, a qualitative description of the sea surface was obtained with a video cassette recorder (VCR).

Subsurface bubble measurements were obtained with a light-scattering technique.² The bubble data acquisition system was suspended from either crane A or B (see figure 2-3), depending on wave direction, currents, and tide. The data were taken at depths between 2 and 21 m below the trough of the prevailing sea condition. This system was capable of measuring individual bubbles with diameters ranging from 10 to 400 microns.

Throughout the entire 5-week period of the experiment, electromagnetic (radar) backscatter measurements of the sea surface were taken. The frequency of the radar was in the K_u band at 14 GHz, and the measurements were taken at a fixed grazing angle of 45 deg with the sea surface. The processed radar data produced relative sea surface backscatter as a function of environmental parameters.

Underwater acoustic measurements were made using a circular transducer as a parametric source and a conventional receiver. The transducer was located 160 m west of the southwest leg of the platform and was mounted 7.75 m above the sea floor on a tower, as shown in figure 2-4.

2.3 ACOUSTIC SENSOR

The major objective of the NOREX-85 experiment was to obtain sea surface backscatter data. Achieving this objective in shallow water is hindered by acoustic multipaths due to source side lobe structure and large insonified areas. To alleviate these difficulties, a parametric source was used because of its inherent narrow beamwidths, broad bandwidths, and low side lobe levels.³

The parametric array was operated at a center frequency (f_0) of 39 kHz. The conventional transmitting voltage response for the sensor can be seen in figure 2-5.

Prior to the experiment, frequency-dependent source level and beam pattern predictions were made with the Moffett-Mellen model for parametric acoustic sources.⁴ A summary of the model results can be found in table 2-1. It should be noted that during the experiment at sea, source level measurements were taken for one range as a function of frequency and drive voltage; the agreement with model predictions was excellent. All calculations involving source level and beamwidth in the computation of scattering strength use the values given in the table.

Table 2-1. Model Results of Source Level and Beamwidth for NOREX-85 Data*

f_D, V θ	18 kHz, 2300 V _{pp}		10 kHz, 2300 V _{pp}		5 kHz, 2400 V _{pp}		3 kHz, 2500 V _{pp}	
	SL	BW	SL	BW	SL	BW	SL	BW
90°	202.5	2.6	204.5	3.1	196.5	3.5	190.1	3.8
75°	202.7	2.6	204.7	3.1	196.8	3.5	190.3	3.8
60°	203.2	2.6	205.2	3.0	197.3	3.5	190.9	3.8
50°	203.7	2.5	205.7	3.0	197.8	3.4	191.4	3.7
40°	204.5	2.5	206.4	3.0	198.6	3.4	192.2	3.7
30°	205.4	2.5	207.3	2.9	199.6	3.3	193.2	3.6
20°	206.8	2.4	208.6	2.8	200.7	3.2	194.6	3.5
15°	207.6	2.4	209.4	2.8	201.8	3.1	195.5	3.4
10°	208.7	2.4	210.4	2.7	202.8	3.1	196.6	3.3

* Symbols: θ = grazing angle (deg), SL = source level (dB//1 μ Pa · m), BW = 3-dB beamwidth (deg), f_D = parametric difference frequency (kHz), and V = drive voltage (V_{pp}).

The sea surface area from which backscattered energy contributes to reverberation is an important factor in obtaining scattering strength values. This area (figure 2-6) may be limited by the beamwidth of the acoustic projector (equation (2-1)) or by the length of the transmitted pulse (equation (2-2)):

Beamwidth Limited

$$A = \frac{\pi h^2}{2} \cdot \frac{\sin(\alpha/2) \cdot \tan(\alpha/2)}{\sin^2(\theta)} \left[\frac{1}{\sin(\theta + \frac{\alpha}{2})} + \frac{1}{\sin(\theta - \frac{\alpha}{2})} \right] \quad (2-1)$$

Pulse Length Limited

$$A = CT \frac{h}{\tan(\theta)} \frac{[\tan(\theta + \frac{\alpha}{2}) - \tan(\theta - \frac{\alpha}{2})]}{2} \quad (2-2)$$

where

C = sound speed (m/s),

T = pulse length (s),

h = depth of transducer (m),

θ = grazing angle, and

α = 3-dB beamwidth.

The areas of insonification were beamwidth limited for grazing angles of 90 to 40 deg and pulse length limited for grazing angles lower than 40 deg.

During the NOREX-85 experiment, the circular array was used as both a parametric source and a conventional receiver (see section 2.2). The receiving sensitivity was between -192 dB/1V/ μ Pa at 3 kHz and -188 dB/1V/ μ Pa at 18 kHz. The beampatterns at four selected frequencies are presented in figure 2-7.

2.4 DATA ACQUISITION AND PROCESSING

The signal generation and data acquisition are described in reference 5. The following section contains only a brief overview.

A flow diagram of the signal generation for the parametric array is shown in figure 2-8. To avoid problems during data analysis (which could be caused by the frequency drift of synthesizers or the flutter and wow of analog tape recorders), all frequencies are referenced (locked) to a 10-MHz signal generated by synthesizer 1. This synthesizer also produces one-half

of the difference frequency $f_0/2$. The $f_0/2$ is gated by an analog switch, which is controlled by a trigger box. The length of the gate is equal to the pulse length. The trigger box also generates a longer gate, which is required for the transmit/receive switch of the parametric array. The half-difference frequency and the center frequency f_0 (which is generated by synthesizer 2) are fed to a mixer, which produces two primary frequencies (f_1 and f_2):

$$f_1 = f_0 + \frac{f_0}{2} \quad (2-3)$$

and

$$f_2 = f_0 - \frac{f_0}{2} \quad (2-4)$$

The mixer has high linearity so that the carrier suppression is greater than 60 dB. To eliminate all other frequencies, especially a dc-contribution, the signal is bandpass filtered before it goes into the power amplifiers for the transducer.

Figure 2-9 is a flow diagram of the receiver analog acquisition system. For short propagation ranges, the energy at the primary frequencies is significantly higher than the energy at the difference frequency. Consequently, the received signal must be bandpass filtered and then amplified so that its dynamic range fits the input range of the following compressor. Basically, a compressor is a logarithmic amplifier that reduces the dynamic range of the input signal. The compressed signal and a controlling signal are recorded on analog tape. The advantage of this technique is that the dynamic range of the received signal is no longer limited by the dynamic range of the analog tape recorder.

For analog-to-digital (A/D) conversion, a clock signal, transmit gate, and sampling frequency are also recorded. The analog signals were converted to digital form for analysis. An expander (which has the inverse function of the compressor) reproduced the received signals. The transmit gate was used to begin the A/D conversion of each individual transmission so that the time series started with the outgoing ping. The sampling frequency ($4f_0$) was also taken from analog tape to avoid a drift between the difference and sample frequency.⁶ This was necessary because the signal envelope had been obtained using a complex demodulation technique.⁷

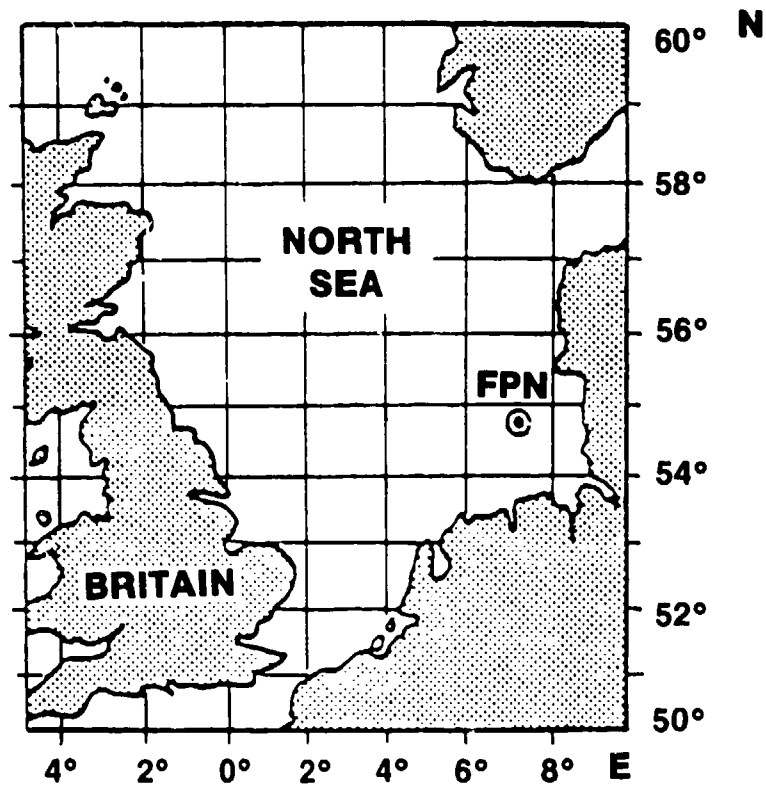


Figure 2-1. Measurement Location

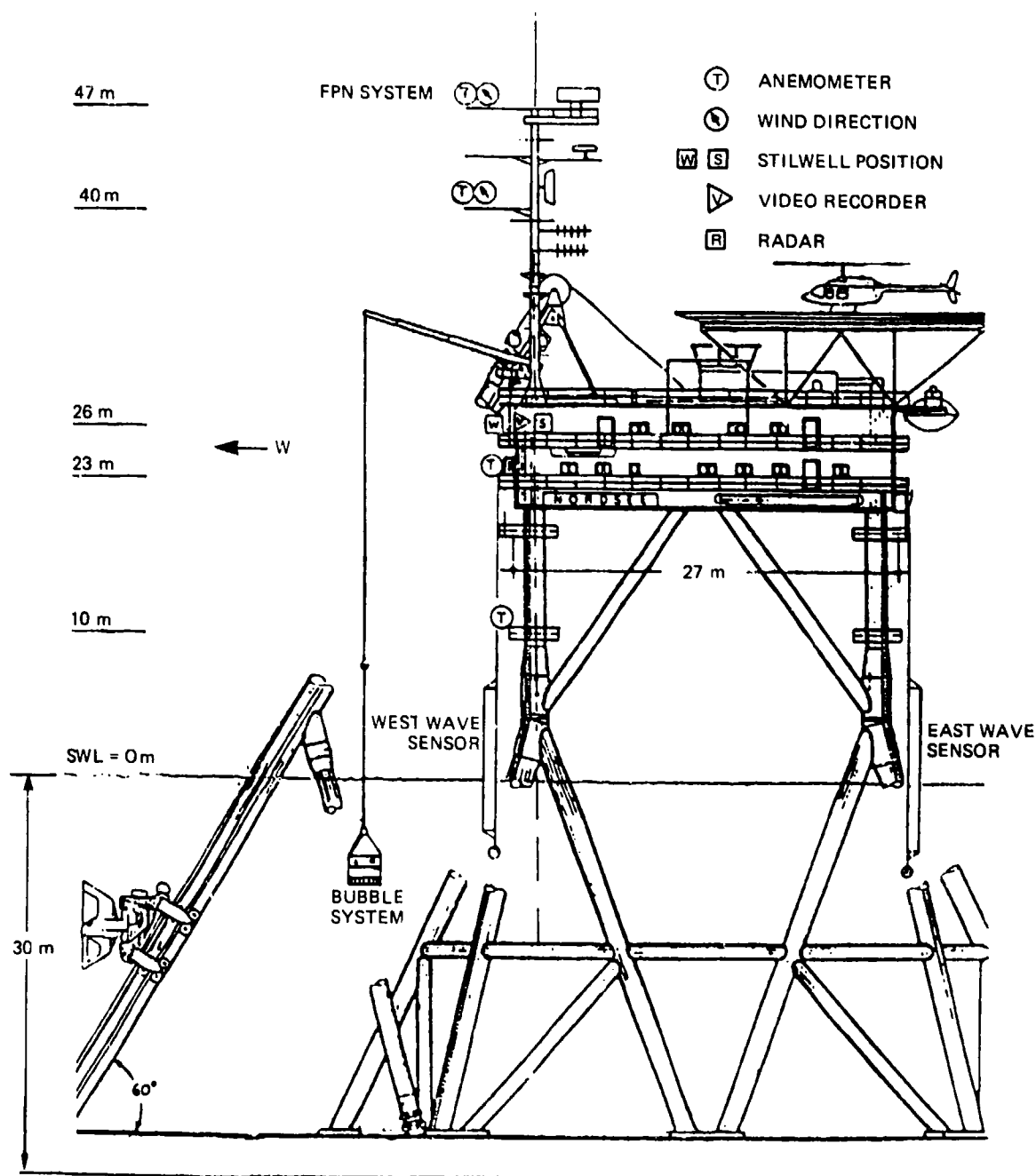


Figure 2-2. FPN Schematic -- Side View

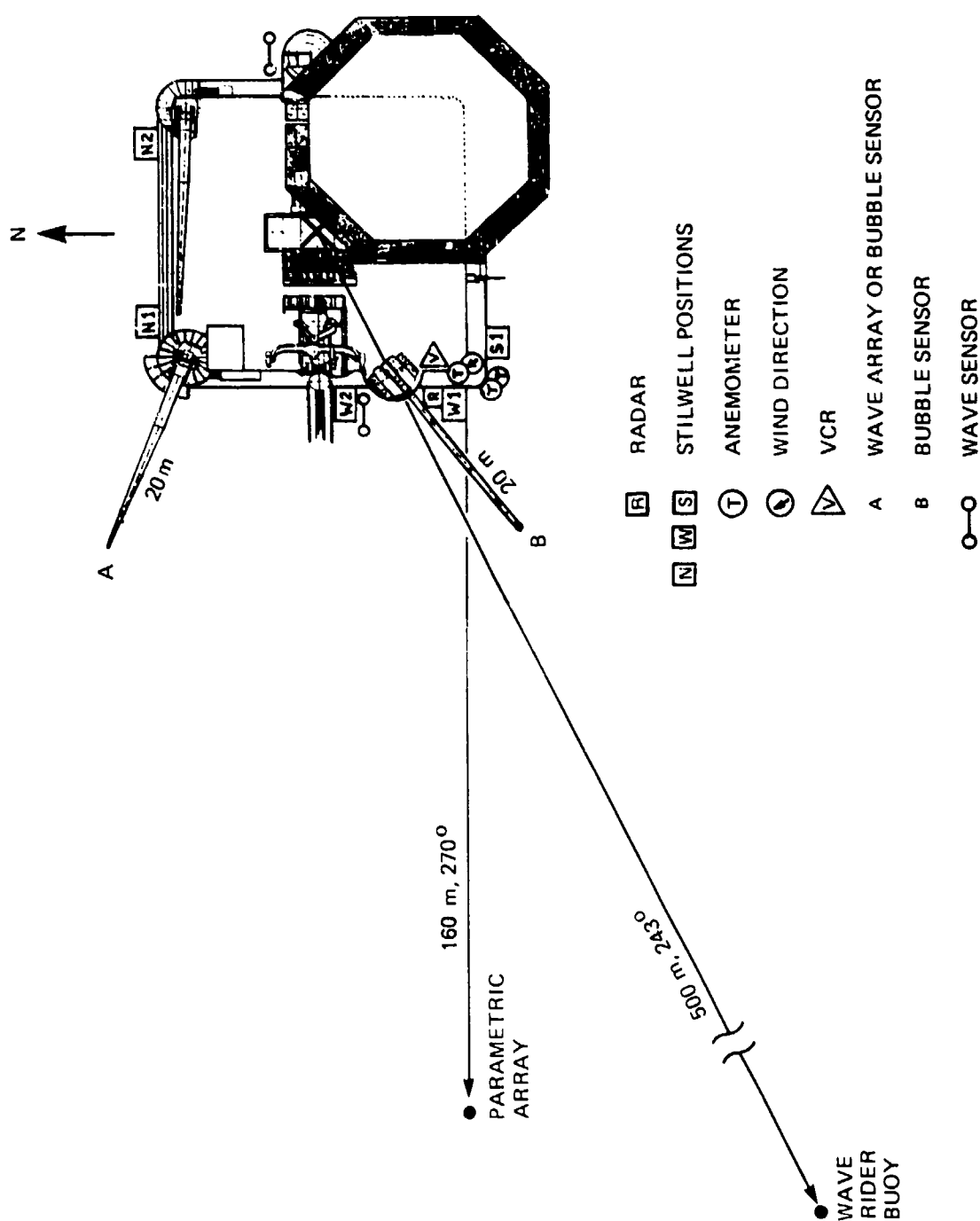


Figure 2-3. FPN Schematic -- Top View

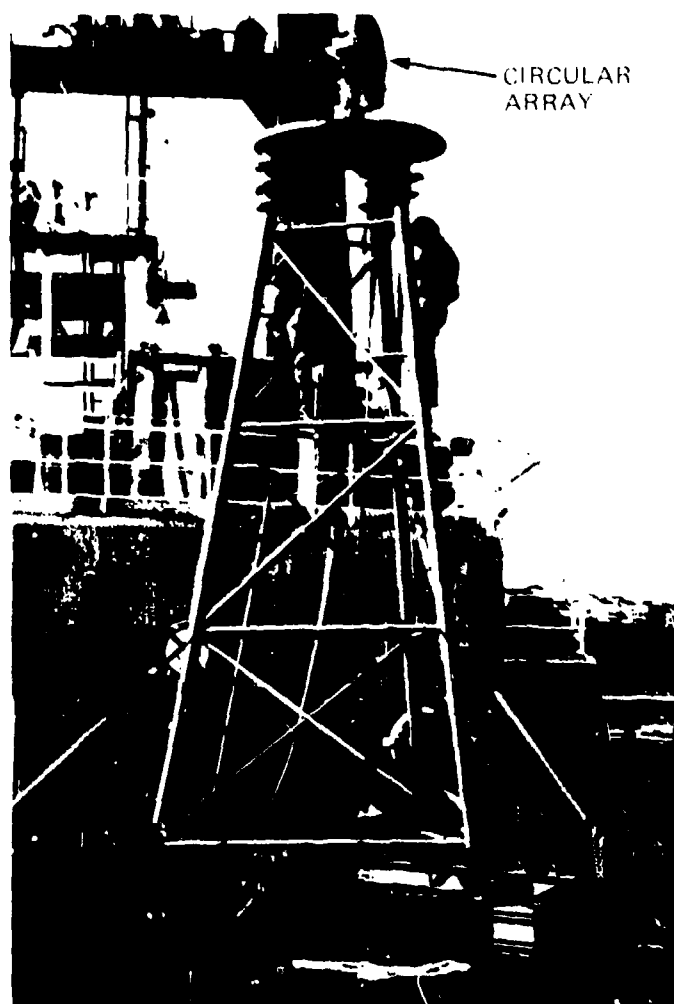


Figure 2-4. Acoustic Sensor and Mounting Tower

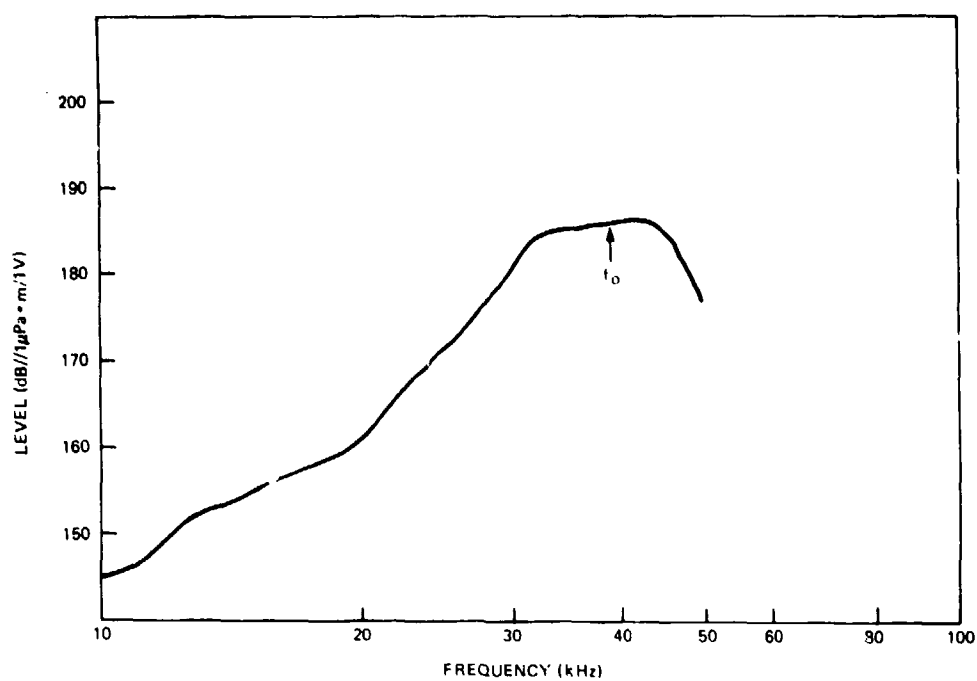


Figure 2-5. Transmit Voltage Response of Acoustic Source

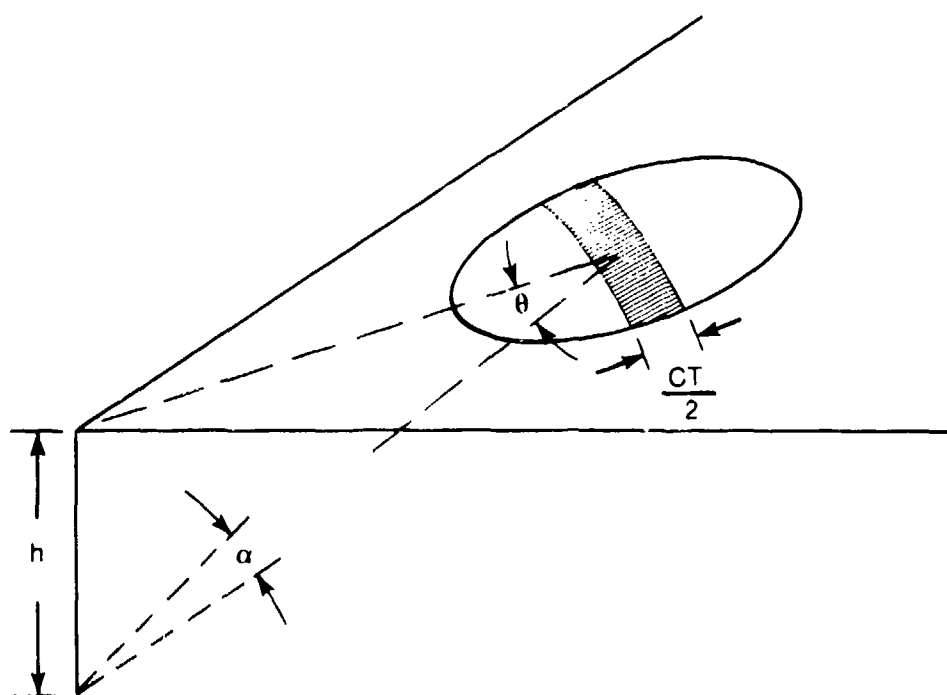


Figure 2-6. Insonification Area

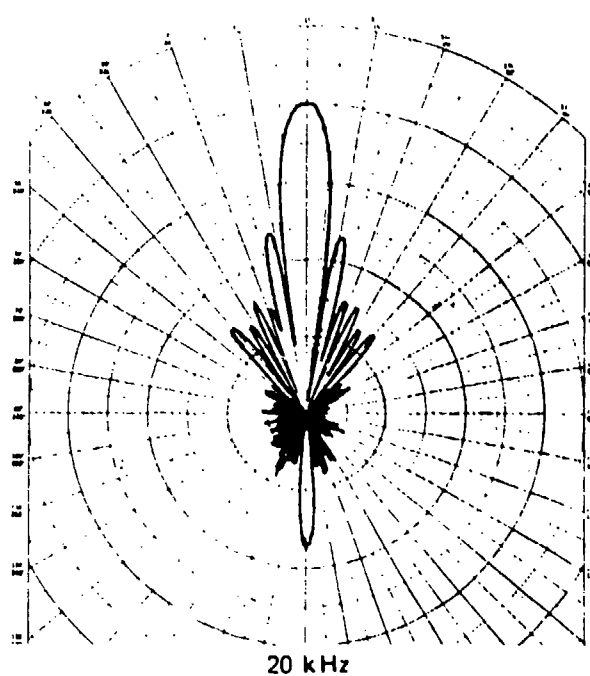
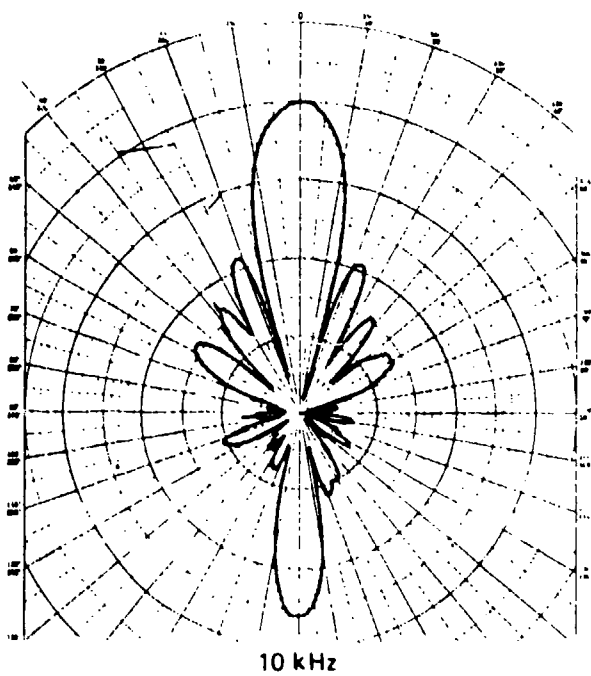
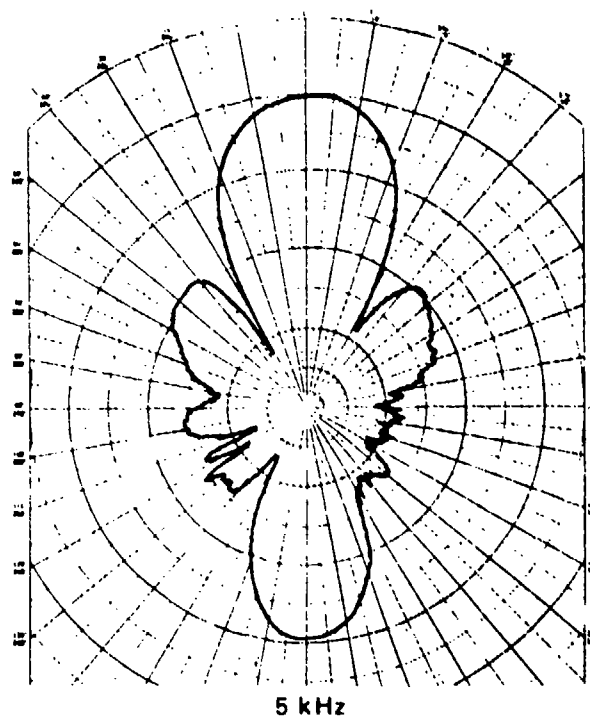
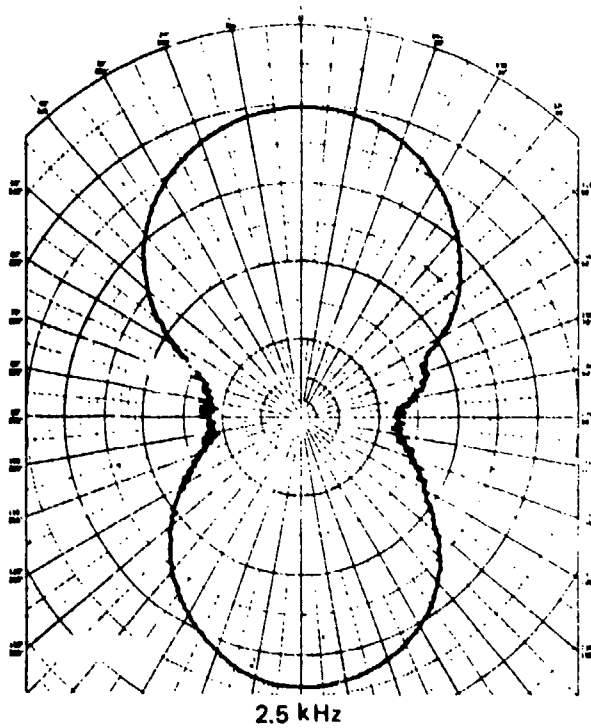


Figure 2-7. Receiving Beampatterns of Acoustic Sensor in Conventional Receive Mode

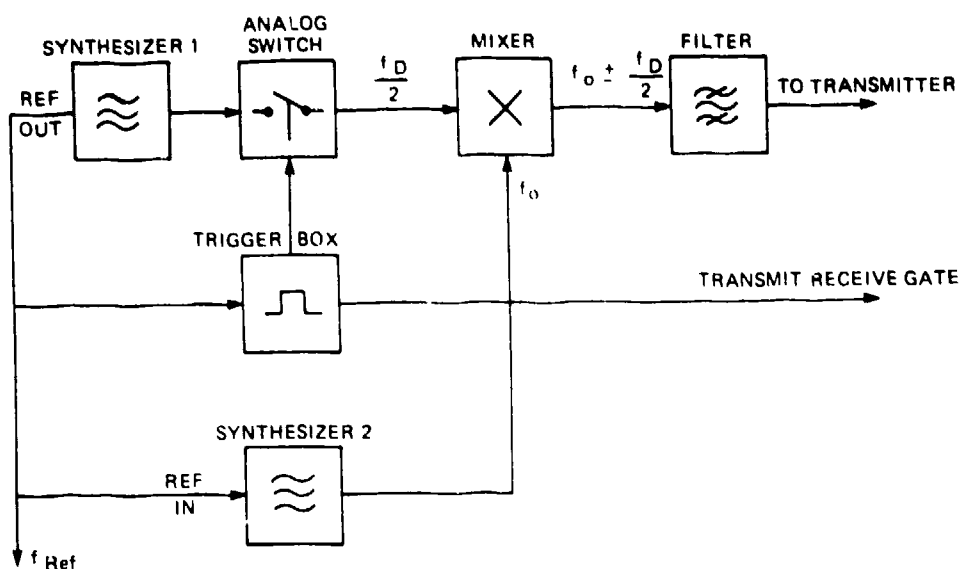


Figure 2-8. Flow Diagram for the Transmit Signal Generation

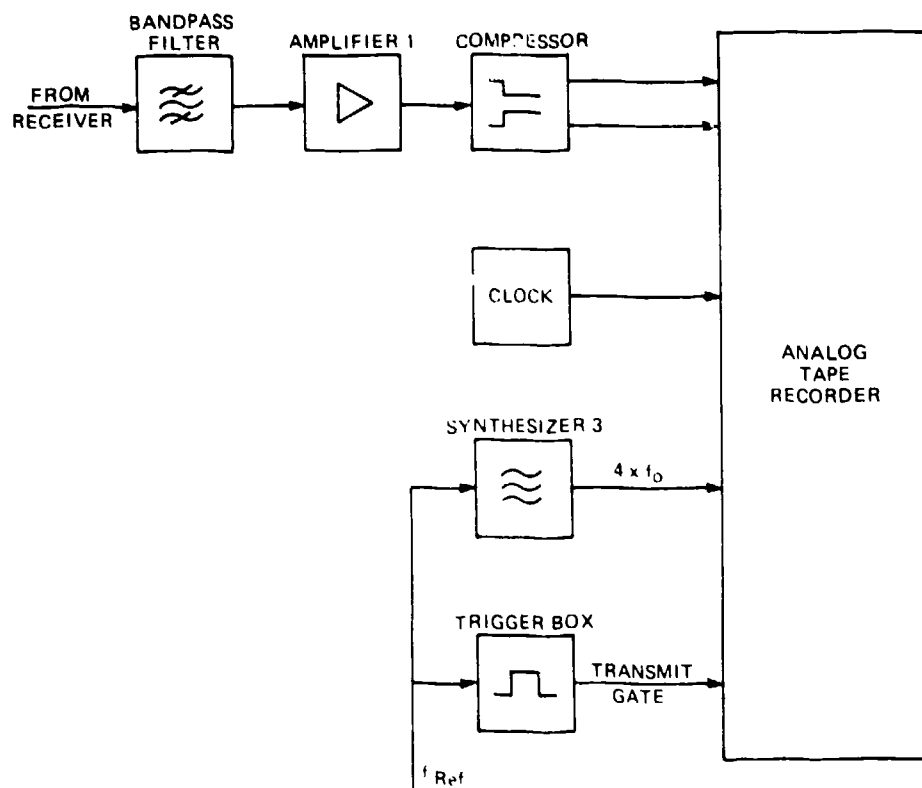


Figure 2-9. Flow Diagram for the Receiving Signal Data Acquisition

3.0 SUPPORTING MEASUREMENTS

The results from previous sea surface acoustic scattering experiments indicate a strong dependence on the environment, particularly at low grazing angles. These studies conclude that this dependence is due to either high frequency ocean wavenumber spectra or subsurface bubbles. During NOREX-85, several diverse supporting measurements were made to correlate the acoustic scattering with specific environmental parameters.

3.1 METEOROLOGICAL

3.1.1 Precipitation

The platform is equipped with sensors to continuously measure rainfall. All types of precipitation are noted every hour by the FPN watch personnel in the platform log. During the experiment, periods of rain, snow, sleet, and hail were noted.

3.1.2 Wind Velocity

Anemometers are mounted at different locations on the platform to measure wind speed and direction. The wind data used for experimental analysis were obtained from an anemometer mounted to the mast of the platform 47 m above the sea surface (see figure 2-2). Wind velocity data (U_{47}) were averaged for 10 minutes. During the 5-week experiment, the 10-minute average wind speed varied from 0 to 49 knots. The maximum wind speed during gusts was 74 knots. The wind speed during measurement sets ranged from 1 to 49 knots so that a wide variety of environmental conditions was encountered.

3.2 OCEANOGRAPHIC

3.2.1 Tides

The average water depth in the measurement area is 30 m. The normal tidal variation is ± 1 m. The water depth is also influenced by wind speed and direction. For example, a persistently strong wind from the northwest forced water to move toward the coast. During this time, the water height was about 33 m at high tide and 31 m at low tide, as shown in figure 3-1.

Because water height influences propagation range and geometry, acoustic source level and transmission loss are tide dependent. To allow in-situ decisions concerning tidal effects, the analog voltage of a pressure sensor, mounted to a platform leg, was monitored in the laboratory. Further analysis showed that tidal effects had a significant influence on acoustic results because the propagation range could be changed about 10 to 15 percent owing to varying water height.

3.2.2 Sound Speed

During the time of year the experiment was conducted, the water in the area is well mixed, which results in a nearly constant sound speed as a function of depth, as shown in figure 3-2. Sound speed was calculated from periodic measures of temperature, salinity, and pressure so that accurate ranges based on propagation time could be obtained. The sound speed changed from 1495 m/s near the beginning of the experiment to 1482.7 m/s at the end of the measurement period.

3.2.3 Sea Surface Characteristics

The broad spectrum of wind velocity caused a wide range of sea state conditions during the experiment. The significant waveheight, $H_{1/3}$, varied during the 5-week period from 0.3 to 7.5 m. The waveheight during measurement periods was between 0.4 and 4.8 m. An experiment similar to NOREX-85 was done in the vicinity of FPN in 1983.⁸ The data analysis showed that a detailed knowledge of the sea surface characteristics is necessary to correlate acoustic results and environmental effects. To provide surface characteristics over a wide range of ocean wave spectra, several different measurement systems and techniques were used.

3.2.3.1 Wave Rider Buoy. Nondirectional sea surface characteristics from the lowest range of the frequency spectrum to about 0.3 Hz are continuously provided by a wave rider buoy. This buoy is 0.7 m in diameter and is located 500 m from FPN. It is secured to the sea floor and the data are telemetered to the platform. These data provide

- analog voltage that is proportional to the waveheight,
- a 10-minute average of the significant waveheight $H_{1/3}$ (longer average times are selectable),
- a plot of the power spectral density averaged over 0.5 hour or 4 hours (selectable), and
- additional statistical information.

Significant waveheight ($H_{1/3}$) is the average of the highest one third of the waves.

Figure 3-3 presents significant waveheight versus wind speed for acoustic measurement sets taken during NOREX-85. As can be seen, there is a broad range of wind speeds for a given significant waveheight. Also shown are three curves representing different simplified wind speed-waveheight models. Curve A represents waveheight as derived from the sea surface spectrum model developed by Pierson and Moskowitz.⁹ This model can be used to predict $H_{1/3}$ for a fully developed sea with the following equation:

$$H_{1/3}(m) = 0.00565[\text{Wind Speed (knots)}]^2 \quad (3-1)$$

Curves B and C are alternative empirical fits to the data to illustrate the inappropriateness of the Pierson-Moskowitz model. Curve B is represented by

$$H_{1/3}(m) = 0.00368[\text{Wind Speed (knots)}]^2 \quad (3-2)$$

and curve C is represented as

$$H_{1/3}(m) = 0.00164[\text{Wind Speed (knots)}]^2 \quad (3-3)$$

The wide range of coefficients makes it apparent that the correlation between significant waveheight and wind speed in the shallow waters of the North Sea is relatively poor. This result is due to intense, rapidly moving low pressure systems coming in from the Atlantic Ocean. The sea state is, therefore, normally duration and not fetch limited.

3.2.3.2 Stilwell Photography. To investigate the effects of high frequency ocean waves on acoustic scattering at the sea surface, the directional ocean wave spectra were to be measured down to wavelengths of about 10 cm. To accomplish this, a photograph of the sea surface was taken and analyzed using Stilwell's technique.¹⁰ In principle, the variations of density of the photographic emulsion are in a first order approximation related to the sea surface slopes. Performance of a two-dimensional Fourier transform of the optical density can obtain a functional relationship to the directional spectra of the inclination of the sea surface slopes. With the assumption of gravity wave theory, this technique, in turn, allows a calculation of the directional energy spectrum of the sea surface. The photographs were analyzed using a digital technique modified by Baur,¹ as shown in figure 3-4. The minimum analyzed frequency is about 1.2 Hz, which is a result of the limited-area coverage of the photograph. The maximum analyzed frequency in this case is 3.8 Hz. Lines of constant wavenumber (or frequency) are concentric circles with the center in the middle of the plot. The contour interval, depicted by the intersection of a black and white stripe, is 6.5 dB.

3.2.3.3 VCR. When acoustic measurements were made during daylight hours, the sea surface was recorded with a VCR. This instrument was equipped with a zoom lens so that the acoustically insonified area on the surface could be recorded.

Relative measurement time was included in the recording. This permitted the sea surface conditions to be related to individual transmissions. From these recordings, qualitative information regarding the occurrence of breaking waves, spindrift, and general surface roughness was obtained.

3.3 BUBBLE MEASUREMENTS

During the experiment an attempt was made to measure microbubbles in the 10- to 400- μ m-diameter range. The measurements were done using a light scattering instrument, which is described in reference 2. The sensor was deployed by a platform crane so that its distance to the platform leg was 30 m or less.

Because it is possible that the data were contaminated by wave interactions with the platform legs and cooling water effluents, the quantitative data obtained from the bubble measuring system were not used.

For the interested reader, results of the bubble measurements are being documented separately.¹¹

3.4 ELECTROMAGNETIC (RADAR) MEASUREMENTS

In addition to the acoustic measurements, electromagnetic (radar) measurements of the backscattering strength of the sea surface were made. The antenna was mounted 22.5 m above mean sea level at the position shown in figure 2-2. The radar data were not calibrated so that only relative data of the electromagnetic backscattering strength of the sea surface are available.

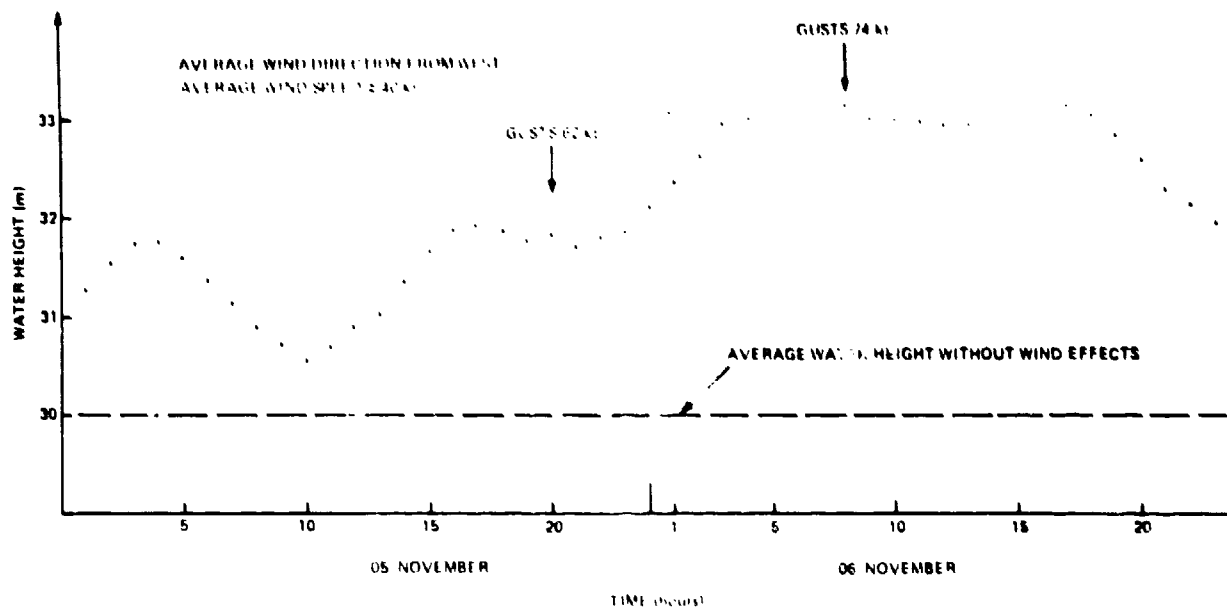


Figure 3-1. Influence of Wind Velocity on Water Height

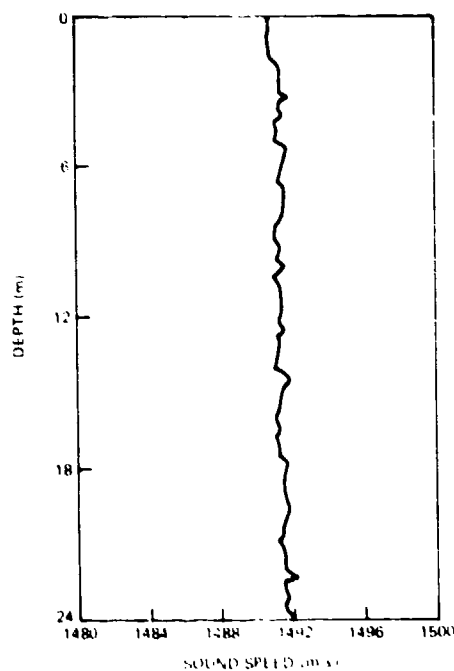


Figure 3-2. Sound Speed Profile on 14 November 1986

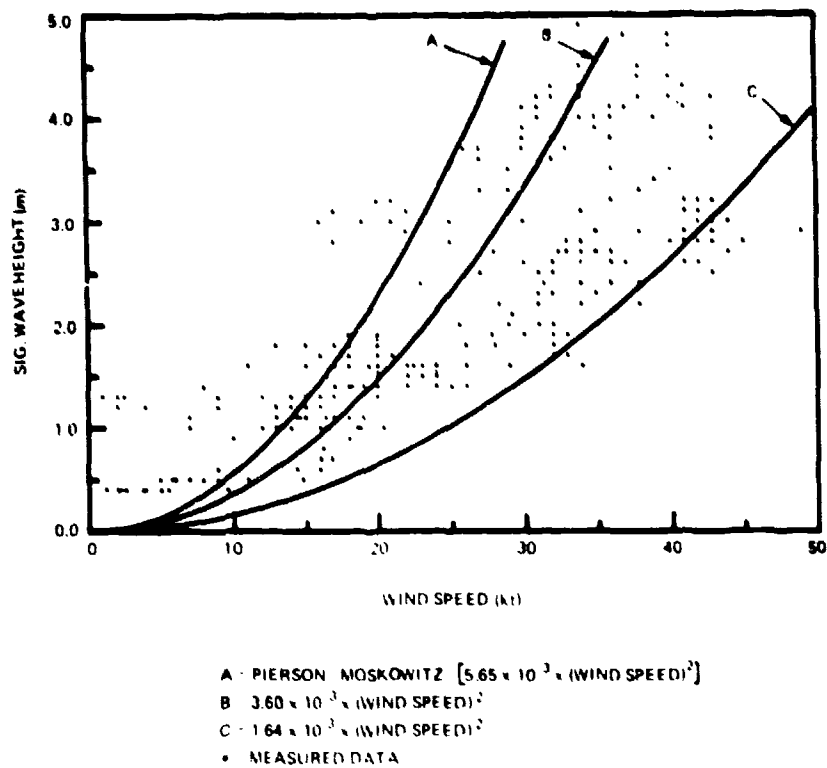


Figure 3-3. Significant Waveheight vs. Wind Speed During NOREX-85

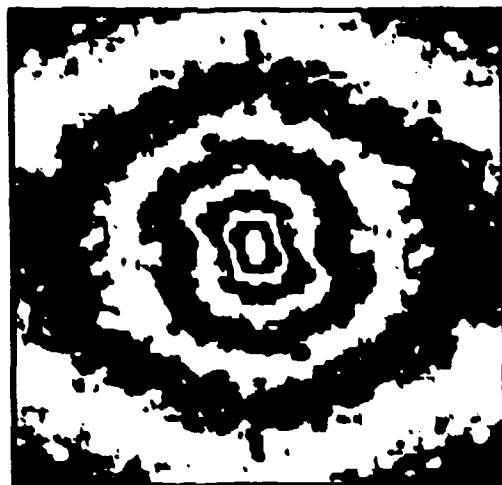


Figure 3-4. Directional Spectrum of the Sea Surface Using Stilwell's Technique

4.0 ACOUSTIC SURFACE AND SUBSURFACE SCATTERING

4.1 THEORY

4.1.1 Background

Numerous theoretical studies and experimental programs have been conducted to investigate acoustic reverberation originating at or near the sea surface. The results of these programs indicate surface roughness and air bubbles must be considered to explain the environmental dependence of acoustic scattering on sonar engineering parameters such as frequency, grazing angle, and system design characteristics.

4.1.2 Incoherent Scattering

The intensity of a scattered acoustic wave is equal to the incident intensity times a scattering function. When the incident and scattered intensities are each modified by a transmission loss coefficient (TLC), we may express the reverberation intensity at a receiver, I_r , arising from an elemental scatterer, i , in terms of intensity at the source, I_o , as follows:

$$I_{r_i} = \frac{I_{o_i} \psi_i}{TLC_{os_i} TLC_{sr_i}}, \quad (4-1)$$

where

TLC_{os_i} = transmission loss coefficient from source, o , to i th scatterer, s ,

TLC_{sr_i} = transmission loss coefficient from i th scatterer, s , to receiver, r , and

ψ_i = elemental scattering cross section.

The total reverberation can thus be represented as a sum over the contributing scattering elements:

$$\sum_{i=1}^N I_{r_i} = \sum_{i=1}^N \frac{I_{o_i} \psi_i}{TLC_{os_i} TLC_{sr_i}}. \quad (4-2)$$

The extent or number of scattering elements may be determined by realizing that the reverberation at any instant of time is a convolution of the spatial impulse response of the scatterers and the transmitted signal.¹²

When the scattering mechanisms are distributed or located such that their temporal extent is greater than the pulse length, the contributing scatterers are determined by pulse length. When the pulse length is longer than the temporal extent of the scatterers, all elemental scatterers may contribute. Instantaneous values of acoustic intensity obtained using the procedure in section 2.4 represent steady state measurements. Furthermore, if we assume that the source intensity is constant over the scattering cross section, we may write

$$I_r = I_o \sum_{i=1}^N \frac{\psi_i}{TLC_{os_i} TLC_{sr_i}} \quad (4-3)$$

Scattering cross sections are not usually presented in sonar literature. Instead, the decibel measure of a scattering function related to target strength is commonly used. For scattering from a surface, the elemental scattering cross section is related to the scatter function by

$$\psi_i = \sigma_i A_i, \quad (4-4)$$

where σ_i is the scattering function for the i th area and A_i is the elemental area. The elemental surface scattering strength, S_{s_i} , is defined to be

$$S_{s_i} = 10 \log \sigma_i = 10 \log \frac{\psi_i}{A_i}. \quad (4-5)$$

The active sonar equations for backscatter from the sea surface may now be obtained by substituting equation (4-4) into (4-3):

$$I_r = I_o \sum_{i=1}^N \frac{\sigma_i A_i}{TLC_{os_i} TLC_{sr_i}} \quad (4-6)$$

For the cases when (1) the transmitter and receiver are co-located, (2) the transmission loss to all contributing scatters is the same, and (3) the scattering function over the insonified area is constant, the above equation may be written as

$$\sigma = \frac{I_r TLC^2}{I_o A} \quad (4-7)$$

or, in terms of the active sonar equation, as

$$10 \log \theta = S_s = RL + 2TL - SL - 10 \log A , \quad (4-8)$$

where

SL = source level (dB),

RL = reverberation level (dB), and

TL = transmission loss = $10 \log TLC$.

Based on the theoretical work of Bass and Fuks,¹³ a two-scale description of the sea surface is needed to characterize the acoustic surface scattering. In this description, the scattering surface is represented as a superposition of small ripples on large waves. The surface backscatter is produced by Bragg diffraction from small wavelets satisfying $K = 2k \cos \theta_g$, where K is the ocean wavenumber, k is the acoustic wavenumber, and θ_g is the local grazing angle. Wavelength is related to wavenumber by $\lambda = 2\pi/K$ (figure 4-1). The large waves cause the Bragg diffraction grating to tilt, thus modifying the average grazing angle, θ .

For an admixture of air bubbles and water, the elemental scattering cross section is related to the scattering function by¹⁴

$$\psi_i = s_{vi} R_0 V_i = R_0 V_i \sum_{j=1}^N N_{ij} \sigma_{ij} , \quad (4-9)$$

where

s_{vi} = backscattering coefficient of volume V_i ,

σ_{ij} = scattering cross section, j -type bubbles in V_i ,

N_{ij} = number of j -type bubbles in V_i ,

R_0 = reference distance, and

V_i = elemental volume in which bubble admixture is located.

The volume scattering strength is defined to be

$$S_v = 10 \log s_v R_0 . \quad (4-10)$$

A combination of equations (4-9) and (4-3) obtains the following sonar equation for backscatter from bubbles:

$$I_r = I_0 \sum_{i=1}^N \frac{R_0 V_{ij} \sum N_{ij} \sigma_{ij}}{TLC_{os_i} TLC_{sr_i}} . \quad (4-11)$$

This equation may be reduced to simpler form only under certain conditions, which may not even be met over short periods in the open ocean. When the bubble layer is relatively thin, the insonified volume small, and the acoustic frequency low, we can expect the transmission loss to each bubble to be constant. Then, we may write the active sonar equation as

$$10 \log \sum_j R_0 N_j \sigma_j = S_v = RL + 2TL - SL - 10 \log V . \quad (4-12)$$

We note that the volume scattering strength is dependent on all bubble sizes and depending on the distribution may not be principally controlled by resonant bubbles. In addition, σ is strongly dependent on acoustic frequency near resonance.

Based on the work by Thorpe and others,^{15,16} bubble density in the ocean is not always horizontally stratified. When the wind is strong enough to form whitecaps, bubble clouds or plumes are generated. These plumes penetrate surprisingly far into the water column, exhibit many different characteristics (similar to cloud formations in the atmosphere), and have fluctuation periods from 1 to 10 minutes.¹⁷ It thus seems appropriate to hypothesize two types of near-surface bubble formations (figure 4-1). One formation consists of uniform layers of microbubbles, which form a background bubble density. The other consists of bubble plumes containing much larger bubbles with very high densities; this formation will exhibit long time variations as the plumes disperse and decay. We would expect acoustic scattering from the uniform layer to appear as a random stationary process. Scattering from plumes using high resolution sonars would exhibit the temporal characteristics of the plumes and would appear as a nonstationary process. These fluctuations decrease for higher wind speeds and higher frequencies. One should note that the contribution of the total backscattering caused by bubbles of larger diameter than the bubble resonance can have a more significant impact on scattering than the resonant bubbles alone (figure 4-2).

4.1.3 Coherent Scattering

The solution of the image reflection problem for the reflection at a plane interface is

$$\phi_{coh} = \frac{I_r}{I_0} \left(TLC_{os} + TLC_{sr} \right) , \quad (4-13)$$

where, as before, TLC_{os} and TLC_{sr} correspond to transmission loss coefficients from the source to surface reflection point and from the

surface point to the receiver. The active sonar equation for specular reflections is

$$10 \log \theta_{\text{coh}} = S_{\text{scoh}} = RL - SL + TL_{\text{or}} , \quad (4-14)$$

where the transmission loss, TL_{or} , is from the source to the receiver. For a homogeneous nonabsorbing medium, TL_{or} is simply related to range r , and at normal incidence when the source and receiver are co-located, the equation is

$$TL_{\text{or}} = 20 \log(2r_{\text{os}}) . \quad (4-15)$$

4.2 MEASUREMENT

4.2.1 Data Set

During the experiment, more than 250 data sets were taken. Scattering measurements were made at the four selected frequencies (3, 5, 10, and 18 kHz) for grazing angles from normal incidence to 15 deg. At 30 and 15 deg, backscattering strength was measured for different sea state conditions in up, down, and crosswave directions. At 60 and 30 deg, backscattering strength was measured at 20-deg azimuthal increments over a 280-deg sector.

Table 4-1 shows the acoustic frequency and the range of significant waveheights, $H_{1/3}$, and wind velocities related to each data set. In addition, the last three rows indicate (1) when recordings of the surface were made with the VCR, (2) when photographs were taken for later Stilwell analysis, and (3) when the scalar (S) or directional (D) spectrum of the sea surface was measured. Each measurement set or event consisted of 750 or 500 transmissions of 4-ms pulses at a repetition rate of 400 ms.

4.2.2 Data Analysis

Even though the number of sonar parameters was reduced to a minimum, different analysis techniques and algorithms were required to process and analyze the data. The methods used were dictated by the grazing angle, the scattering process, and the need for individual or ensemble-averaged results.

When the area contributing to backscattered energy is limited by the projector beamwidth, as is the case for grazing angles between 90 and 40 deg, the time shift of the received surface echo due to waveheight can be larger than the pulse length. For these grazing angles, each return is time shifted so that the leading slope of the surface echo always appears at the same time. The time-shifted pulses are then summed to obtain ensemble-averaged results. At lower grazing angles, when the contributing area is pulse length limited, the peak reverberation level within a time window related to the grazing angle is used to compute scattering strength.

Equation (4-8) was used to compute backscattering strength from reverberation level at all grazing angles except 90 deg. Equation (4-14)

Table 4-1. NOREX-85 Data Set

Event No.	Frequency (kHz)	Wind Speed (knots)	Wind Direction (deg)	Waveheight $H_{1/3}$ (m)	VCR	Photo	Waves
1400-1408	18	27-37	320	3.7-4.8	✓	✓	
1409-1418	18	17-27	320	2.4-3.6			
1419-1428	18	40-43	220	3.5-4.8	✓	✓	S
1429-1437	10	32-40	220	3.6-4.5	✓	✓	
1438-1446	5	32-36	230	3.8-4.2	✓		
1447-1455	3	29-39	230	3.5-4.1			
1456-1464	2	16-29	240	3.0-3.2			
1465-1473	18	1-9	changing	1.2-1.4	✓	✓	D
1474-1475	10	8-9	150	1	✓	✓	
1476-1485	18	7-9	150	0.5-0.6	✓	✓	S
1486-1490	10	6-7	170	0.5	✓	✓	S
1491-1495	5	6	175	0.5	✓	✓	S
1496-1500	3	5-7	170	0.5	✓	✓	S
1501-1509	10	17-24	135	1.3-1.5	✓	✓	D
1510-1518	5	15-19	150	1.2-1.4	✓	✓	D
1519-1527	3	14-16	150	1.1-1.3			D
1528-1534	10	23-26	80	1.4-1.6	✓	✓	D
1535-1541	5	24-34	73	1.4-1.8	✓	✓	D
1542-1548	3	32-33	75	1.7-2.0	✓	✓	D
1549-1555	18	42-44	83	2.7-3.2	✓	✓	D
1556-1562	10	41-49	83	2.8-3.0	✓	✓	D
1563-1569	5	41-43	80	2.6-3.2	✓	✓	D
1570-1576	3	39-41	80	2.8-3.4	✓	✓	D
1577-1585	10	30-45	80	2.2-3.2			D
1588-1596	3	12-15	90	1.1-1.3	✓	✓	D
1598-1606	5	13-19	90	1.1-1.2			D
1609-1617	10	12-17	90	1.0-1.1			D
1621-1629	3	2-5	240	0.4	✓	✓	D
1632-1633	5	15	260	0.5-0.6			D
1634-1635	10	16	270	0.6-0.7			D
1639-1647	18	11-20	300	1.6-1.9	✓	✓	D
1648-1656	3	13-23	300	1.6-1.8	✓	✓	D
1661-1665	18	30-34	0	1.9-2.4	✓	✓	D
1666-1670	10	34-38	0	2.2-2.4	✓	✓	D
1671-1677	5	34-43	0	2.5-3.1	✓	✓	D
1678-1688	3	28-37	0	3.2-3.3	✓	✓	D
1701-1711	3	30-31	140	2.0-2.5	✓	✓	D
1718-1733	3	20-21	240	1.5-1.9	✓	✓	D
1734-1748	3	34-36	220	2.4-2.9	✓	✓	D
1749-1764	3	34-36	220	2.4-2.9	✓	✓	D

was used to compute coherent scattering strength or reflection loss from backscattered energy at the 90-deg grazing angle.¹⁸

4.3 BACKSCATTER RESULTS

4.3.1 Saturation

Figure 4-3 shows the measured backscatter strength as a function of grazing angle for two frequencies at relatively high wind speed conditions. These data illustrate that, for a given acoustic frequency, there appears to be a wind speed or waveheight above which the backscattered energy no longer increases; that is, saturation occurs. From this figure, we can see that saturation occurs at all grazing angles and that the saturation value of the backscattering strength is higher at lower frequencies.

To investigate the onset of saturation, the backscattering strength is shown as a function of wind speed for 3 and 18 kHz at grazing angles of 30 and 15 deg in figures 4-4 and 4-5. Although the backscattering strength shows a strong temporal variability, as will be described in a later section, the general trend is related to the wind speed or the waveheight. As expected, the backscattering strength increases with increasing wind speed. As can be seen from both figures, there is a frequency and grazing angle dependence for the saturation onset. At a grazing angle of 30 deg, the saturation begins at about 40 knots of wind for the 3-kHz data and at about 18 knots for the 18-kHz data. For a grazing angle of 15 deg, the saturation onset for 3 kHz is at about 35 knots and for 18 kHz it is at 15 knots. Thus, the saturation onset is at lower wind speeds for higher frequencies and lower grazing angles. Garrison, Murphy and Potter¹⁹ measured a saturation onset at 14 knots of wind for an acoustic frequency of 60 kHz, which is the same trend shown by the present data.

There are two possible explanations for the saturation effect:

- Surface slopes increase with wind speed until a transition to breaking waves occurs; the steepness of the waves is then independent of wind speed.
- The backscattering is caused by bubbles that have their origin in breaking waves; the number of bubbles increases until a uniform maximum density (which masks the surface) is reached.

The authors of this report expect the second scattering mechanism to cause the saturation at the lower grazing angles. Saturation at high grazing angles is due to surface roughness.

We also note in figures 4-4 and 4-5 that the backscattering strength decreases for very high wind speeds at 18-kHz acoustic frequency. We assumed in the data reduction process that the transmission loss is only range dependent. Previous measurements at the same location show a sudden very strong increase in transmission loss with increasing wind speed, which is assumed to be caused by bubbly layers.²⁰ An increase in transmission loss would result in a smaller receiving signal, which would translate to a lower backscattering strength. Thus, we believe that this effect could be caused by the processing technique.

4.3.2 Grazing Angle Dependence

Shown in figure 4-6 are measured values of acoustic backscatter strength (as defined by the incoherent scattering equation near the top of the figure) versus grazing angle for 3, 5, 10 and 18 kHz. Each data point is an ensemble average of about 750 pings obtained during a 5-minute period. A measurement set was obtained at all angles for a given frequency, then the frequency was changed, and the process was repeated. There is only about a 10-minute time lapse between data points connected by straight lines. These data represent backscatter strength at relatively high wind speeds, specifically the 30- to 40-knot range. We can see that there is a dependence on frequency, with higher values of backscatter obtained at the lower frequencies.

Another objective of the experiment was to obtain backscattering strength data over a wide variety of environmental conditions. Shown in figure 4-7 are some of the data that illustrate what we believe comes close to placing upper and lower bounds on backscatter strength at 10 kHz. The wind speed in knots associated with each data point is indicated by the adjacent number. We can easily see that the absolute level and slope of the curves with the highest wind speeds represent saturation values that will not be exceeded unless additional phenomena become important. The curve for the lowest values of wind speed is not quite as definitive because of the limited number of data points, and although the wind speed was almost zero, the significant waveheight during the measurement set was 1.2 m. Thus, we would expect even lower values for a perfectly flat surface.

An important factor in characterizing backscattering as a function of grazing angle is sea surface roughness. The surface roughness is usually considered as composed of (1) a large scale component (the significant waveheight) and (2) a small scale component (ripples and capillary waves). It is usually assumed that the large scale waves are the dominant factor at high grazing angles. As lower grazing angles are approached, the effect of the small scale roughness increases significantly.

During one measurement set at 3 kHz, the wind speed increased from 2 to 5 knots. This increase changed the sea surface from glossy to one covered with small ripples. The significant waveheight was constant at 0.4 m. The upper curves show backscattering strength as a function of grazing angle for these two conditions. At normal incidence the backscatter strength for the glossy surface is about 6 dB higher than for the case where ripples are present. For lower grazing angles, the ripples cause higher backscattering, such that at 60 deg the difference is about 8 dB. During these measurements, photographs of the sea surface were taken and analyzed using Stilwell's technique. The results of this analysis (lower part of figure 4-8) show the associated directional wave spectra. The analysis bandwidth presented is from 1 to 3 Hz. The contour interval, depicted by the intersection of a black and white stripe, is 6.5 dB. The vector U shows the wind direction and ψ indicates the azimuthal orientation of the acoustic axis. The inner circle is drawn for a surface wavelength of 0.25 m, which corresponds to one-half the acoustic wavelength at 3 kHz (see section 4.1.2). The energy of the waves at this frequency in the direction of the acoustic axis is about 10 dB higher when ripples are present. It is expected that the difference between the backscatter values would become

greater for lower grazing angles, as indicated by the different slopes of the two backscatter curves.

4.3.3 Frequency Dependence

Figure 4-9 illustrates the dependence of backscatter strength on frequency at high wind speeds. We can see for the prevailing sea conditions a notable decrease in backscattering strength as frequency increases for the higher angles. This dependence becomes almost nonexistent at the lower grazing angles. A set of similar curves for lower wind conditions is shown for two grazing angles by the dashed lines.⁸ Upon comparing the data near 30 deg, we can see that there is little dependence on frequency in both wind categories. However, at 75 deg there is a considerable difference in the frequency dependence for the two wind conditions. Note the backscattering strength at 75 deg and near 18 kHz is approximately the same for wind speeds of 18 and 40 knots.

4.3.4 Specular Point

Figure 4-10 illustrates normal incidence sea surface backscatter as a function of significant waveheight and wind speed at four frequencies. Backscattering at normal incidence is considered here to be a coherent process.

At 18 kHz it can be seen that backscatter strength decreases as wind speed increases up to about 30 knots. Beyond this wind speed, it appears that saturation is reached and there is no longer any significant correlation between backscatter and wind speed. The difference in the data at 3 kHz is due to a strong dependence on very low wind speeds. This dependence is to be expected because the Rayleigh roughness parameter is small for small areas at low frequencies. Had the experimental data at 18 kHz extended to comparable low wind speeds, we would expect the same trend. For high wind speeds, the scattering strengths at 3 and 18 kHz are similar until the wind speeds are above 28 knots; then the scattering strength again shows a dependence on wind speed, attaining saturation in the 38-knot region. The data at intermediate frequencies exhibit the same trend. It appears that other phenomena must be playing a significant role in the backscattering mechanism.

During the experiment, some periods of rain coincided with the acoustic measurements. Figure 4-11 illustrates the backscattering strength of the sea surface when rain is present for an acoustic frequency of 3 kHz. We immediately notice that for a similar wind speed (32 knots), the backscatter strength increases by 6-8 dB when rain is present.

4.3.5 Temporal Variability

A major objective of the experiment was to determine the environmental and frequency regimes over which acoustic scattering near the sea surface is principally dependent on air bubbles or the roughness of the air/sea interface. Figure 4-12 shows the envelope of two different returns at

normal incidence. The transmitted frequency was 18 kHz with a pulse width of 4 ms. The significant waveheight was 3.3 m and the wind speed was 27 knots. During this time period, many breaking waves occurred. The upper figure shows a single ping return 49 s after the measurement set started. As seen from the steep slope at the beginning of the echo, there is no obvious bubble reverberation. The lower plot, which shows the return from another ping 80 s later, indicates the presence of bubbles down to about 2 m below the surface. To investigate the influence of bubbles on the sea surface backscatter for normal incidence, the reverberation levels received from the surface and from the bubbles were evaluated for each individual ping. The time history of the reverberation level is shown in figure 4-13. The surface reverberation levels are the average over the 4 ms past the very steep slope. The bubble reverberation level is the average over the 1 ms starting 1.6 ms before this slope.

The circles in this figure indicate the levels that correspond to the two pulses in figure 4-12. The time series is 300 s and is a result of 750 pings at a repetition rate of 0.4 s. It can be seen that there is no correlation between surface reverberation and bubble reverberation levels at normal incidence. The reverberation from the surface has a relatively stationary mean. The reverberation level from the bubbles is considerably lower in amplitude and exhibits slowly varying characteristics of much longer time duration than those associated with any wave components. This reverberation level indicates the generation of bubble patches (probably caused by breaking waves) that remain below the surface for an extended period of time.¹⁶

The envelopes of two time series averaged over 750 pings are shown in figure 4-14 for different wind and wave conditions. In both cases the transmit frequency was 18 kHz. The arrival time difference of the individual echoes caused by differing waveheights was removed using a thresholding technique. The upper curve shows the average return for a wind speed of 9 knots and a significant waveheight of 0.5 m. The nearly constant steep slope of the leading edge indicates that there is no apparent scattered energy from a subsurface bubble layer. The lower curve is the average from a high sea state condition. The onset of scattered energy corresponds to a depth of about 3.5 m below the surface. The reverberation level increases until the difference between surface and subsurface scattered energy is about 28 dB. We may thus conclude that at normal incidence and 18 kHz, bubbles are not a dominant scattering mechanism for winds up to at least 27 knots. They do, however, contribute to the total reverberation level at the receiver.

An attempt was made during the experiment to investigate the azimuthal dependence of backscattering relative to wave direction. Three measurements were taken at grazing angles of 30 and 60 deg at 3 kHz. During each measurement, the environmental conditions did not change. For each event, only the azimuthal angle was changed in steps of 20 deg. The time gap between the beginning of two events was about 5 minutes.

The results for these measurements are shown in figure 4-15. All three curves show strong fluctuations in the backscattering strength. The highest difference is 16 dB for the two events marked by crosses in 4-15(c).

Backscatter fluctuations are expected to be caused by

- low frequency waves,
- high frequency waves, and
- bubbles.

Recently developed models,²¹ based on a two-composite roughness theory, assume that backscattering for high grazing angles is caused by low frequency waves and for low grazing angles by high frequency waves. The measurements for 30- and 60-deg grazing angles represent these two different regions. To investigate the high degree of variability from one event to another, the time history for two contiguous events was investigated on a ping-to-ping basis. The backscattered energy from 500 individual pings was evaluated at a fixed time when the maximum echo from the sea surface occurred. The relative backscattered levels (which are not corrected for source level, transmission loss, and insonified area) are shown in figure 4-16. The upper and lower curves correspond to the backscattering strength values marked with a cross in figure 4-15. Curves obtained using this technique for other frequencies at a 30-deg grazing angle all show the same trend when the significant waveheight is 1 m or higher. The backscattered energy suddenly increases by 20 dB or more and stays high for some seconds or minutes. It is obvious that the backscattering strength is affected by the fluctuations, i.e., the value and the duration of high backscatter periods. Until now we assumed that backscattering is a stationary process, but, as can be seen from figure 4-16, mean and standard deviations of the backscattered energy show strong fluctuations when the time series is split into segments of equal length. To increase the integration time, the time series of three events taken in temporal sequence were analyzed, assuming that the sea state conditions did not change significantly over this 15-minute period. From these data, the coefficient of variation c_r , also known as the normalized standard error, is estimated as²²

$$c_r = \frac{\delta}{\mu},$$

where δ is the standard deviation and μ is the mean.

The coefficients of variation as a function of wind speed are shown in figure 4-17 for three frequencies. For very low wind speeds, the coefficient of variation approaches the theoretical value for a Rayleigh distribution of 0.52. The Rayleigh distribution is obtained after squaring data that are Gaussian distributed. The squaring process is accomplished when the envelope of the signals is computed. The coefficient of variation then increases with wind speed for an intermediate region and decreases somewhat again for high wind speeds. It is noteworthy that the intermediate region shows a strong frequency dependence. It continues up to 40 knots at 3 kHz, to 35 knots at 10 kHz, and to 18 knots at 18 kHz. For even higher wind speeds - above the intermediate region - the coefficient of variation stays constant. This is analogous to the saturation curves discussed in an earlier section.

To understand more about the physical process causing the backscatter fluctuations, figure 4-18 shows a sequence of time histories of the 3-kHz data used in computing the coefficient of variation for increasing wind speed. As can be seen, there are almost no fluctuations at the lowest wind speed. At higher wind speeds, which represent the intermediate region from figure 4-17, high backscatter periods are present. The high levels during these periods do not change much with increasing wind speed, but the higher the wind speed is, the longer they stay. A comparison of the curve for wind speeds at 14 and 41 knots shows an almost inverse behavior. At the lower wind speed, there are short high backscatter periods while at the higher wind speed, the backscatter strength drops down only for short periods.

At high wind speeds especially, the backscatter strength remains high for times that are too long to be correlated with the long ocean wavelengths. A correlation with bubbles includes some problems. The curves are shown for an acoustic frequency of 3 kHz. The corresponding bubble radius for resonant scattering is approximately 1.1 mm. These bubbles are too big to be measured with the optical bubble sensor. On the other hand, bubbles of this diameter can only be caused by breaking waves and this information should be available on VCR tape. The qualitative correlation could be done for each individual ping because the actual measuring time was also displayed on tape. The result is that, in most cases, breaking waves occurred at the acoustically insonified area when the backscattering was high. In almost each case, when the time history of the backscattering strength shows a very sharp onset of high backscatter periods, a breaking wave could be seen in the small measuring area. As discussed in an earlier section, it was expected that bubbles would contribute to the reverberation for these high sea state conditions. However, an additional effect seems to influence the backscattering strength. As illustrated in the upper left curve of figure 4-18, there exists a period of high backscatter when the significant waveheight was only 0.5 m. The VCR tape showed that there were no breaking waves present when the data were taken. A possible explanation is given by Middleton and Mellen,²³ who propose that wind-generated solitons, moving nondispersively on the wind-driven drift layer of wind-excited wave surfaces, are a plausible mechanism for large backscatter returns in the absence of near-surface bubble layers. To prove this, the wind stress at the acoustically insonified surface (which could not be measured during the experiment) has to be known.

We may thus conclude that for a grazing angle of 30 deg and an acoustic frequency of 3 kHz, there is a transition from one scattering phenomena to another. All indications lead us to the conclusion that the principal mechanism at low wind speeds is Bragg scattering from the sea surface and the principal mechanism at very high wind speeds is volume scattering from localized bubble concentrations in the form of plumes or clouds and not necessarily from resonance-size bubbles.

To determine the frequency and environmental regimes over which one or the other mechanism is dominant, a subjective analysis of each time series was made to determine the relative period of time each mechanism appeared to be dominating the total scattering strength (figure 4-19). In this figure, region III corresponds to frequencies and winds in which volume scattering from near surface bubbles is the dominant mechanism at least 80 percent of the time. Region I corresponds to frequencies and wind speeds in which

surface scattering is the dominant mechanism at least 80 percent of the time. Region II is a transition region, with the dashed line corresponding to equal time periods of surface and bubble scattering. Because the method used to determine relative time periods is subjective, a sample of each region at 10 kHz is shown in figure 4-20. Figure 4-20(c) is a time series where high values of scattered energy corresponding to volume reverberation are present about 80 percent of the time. Figure 4-20(a) is nearly the opposite case. Here the wind speed is only 7 knots and we can note only two periods of high backscatter near the beginning and end of the record. In this case, an estimate was made that reverberation was the result of surface scattering 90 percent of the time.

4.4 COMPARISON WITH THEORY AND OTHER MEASUREMENTS

As discussed in previous sections, the backscattering is assumed to be caused by bubbles for the high sea state conditions at low grazing angles. Comparable measurements are mostly in higher frequency regions. However, some general trends can be compared as was done for the saturation of backscattering strength. Figure 4-21 shows a comparison between the current data and a combined semiempirical Chapman-Harris²⁴ and Eckart algorithm for a backscattering strength model as a function of grazing angle at a frequency of 10 kHz. Both indicate increasing backscattering strength with wind speed, although differences up to 10 dB are seen.

A theoretical model based on the composite-roughness theory was developed by McCammon and McDaniel²¹ and a comparison with the same data set is shown in figure 4-22. As can be seen, the model underestimates the measured values for all grazing angles. The difference between the measured and predicted data is about 5 dB for a wind speed of 17 knots. For the high wind speed case of 42 knots, the model underestimates the measured data about 15 dB. Obviously, the comparison with this model is not valid if the dominating backscattering mechanism is due to bubbles. Thus, these data are compared with a model from McDaniel and Gorman, which predicts the reverberation from a near-surface homogeneous bubble layer,²⁵ as illustrated in figure 4-23. In addition, this figure contains measured backscattering strength data²⁵ for an acoustic frequency of 20 to 25 kHz. Our data are shown for a frequency of 18 kHz. The different wind speeds are not important because for all wind speeds the data are in the saturation region.²⁶ The model shows general agreement with the data; the two measurements show excellent agreement. The model supports the assumption that the bubbles cause the backscattering for the given frequency and wind speed regime.

Further comparison of NOREX-85 data to other experimental data or theoretical models is difficult because of the lack of published information that is applicable to our data set.

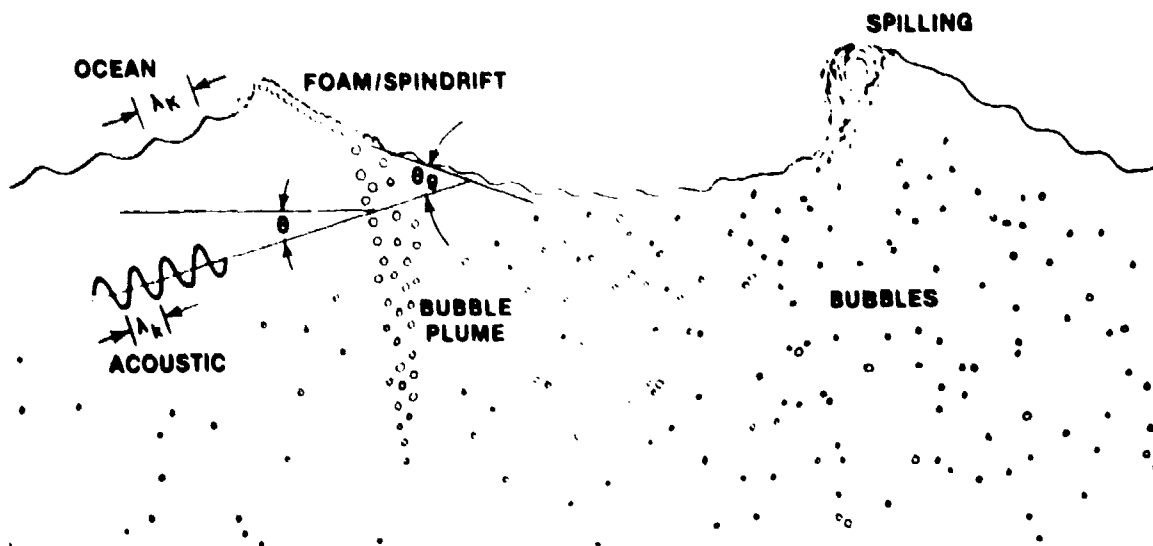


Figure 4-1. Principal Features Affecting Acoustic Surface Scattering

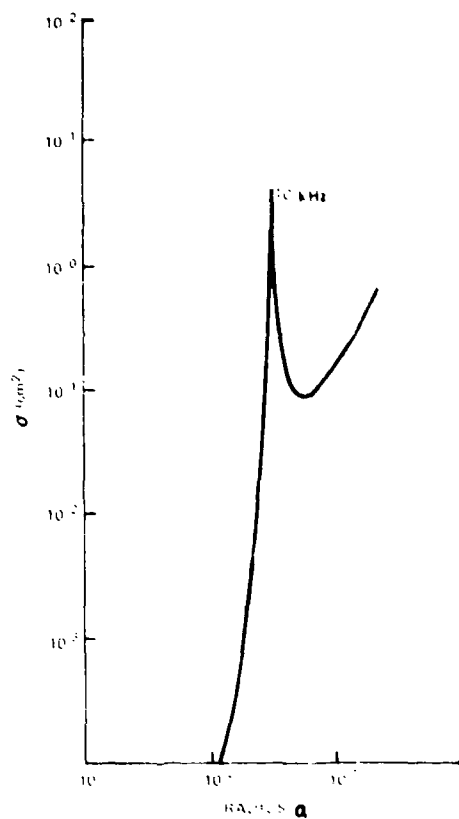


Figure 4-2. Scattering Cross Section of Air Bubbles at 10 kHz

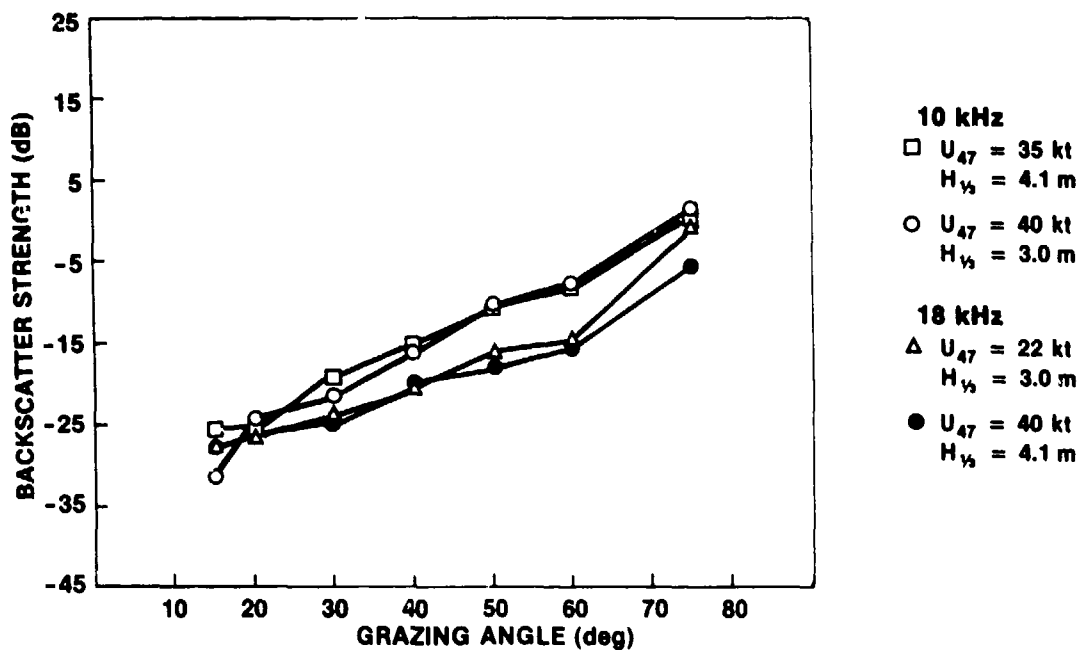


Figure 4-3. Sea Surface Backscatter vs. Grazing Angle (Saturation)

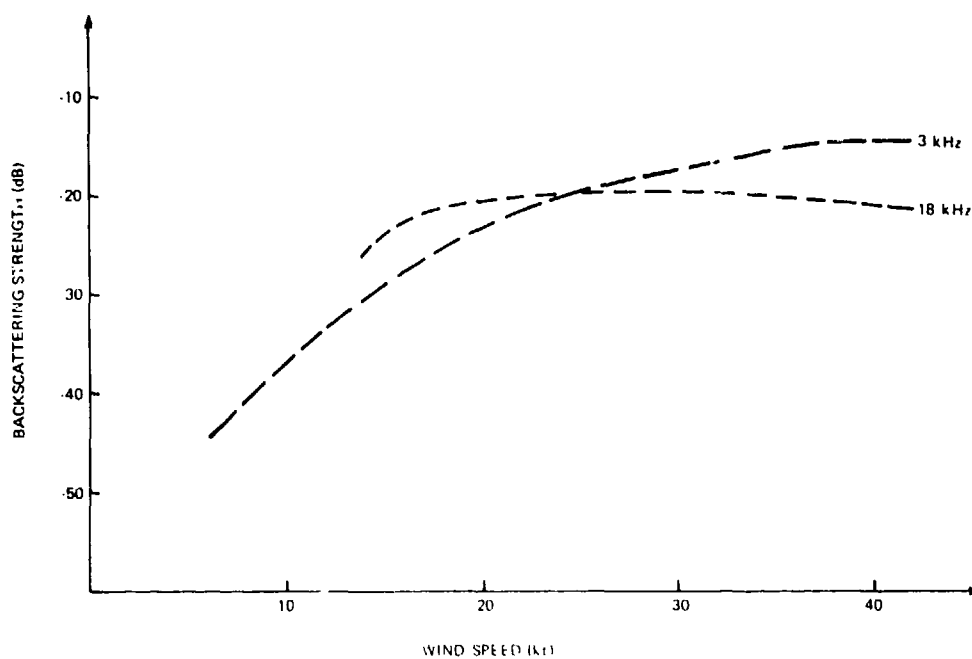


Figure 4-4. Backscatter vs. Wind Speed for a 30-deg Grazing Angle (Frequency Dependence of Saturation Onset)

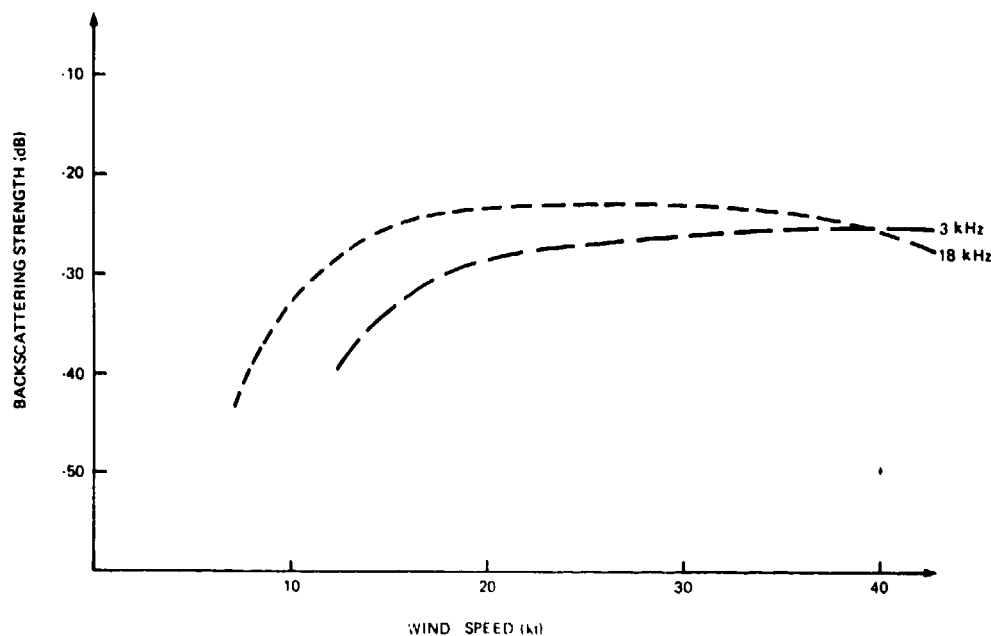


Figure 4-5. Backscatter vs. Wind Speed for a 15-deg Grazing Angle
(Frequency Dependence of Saturation Onset)

$$BS = RL - SL + 40 \log R - 10 \log A$$

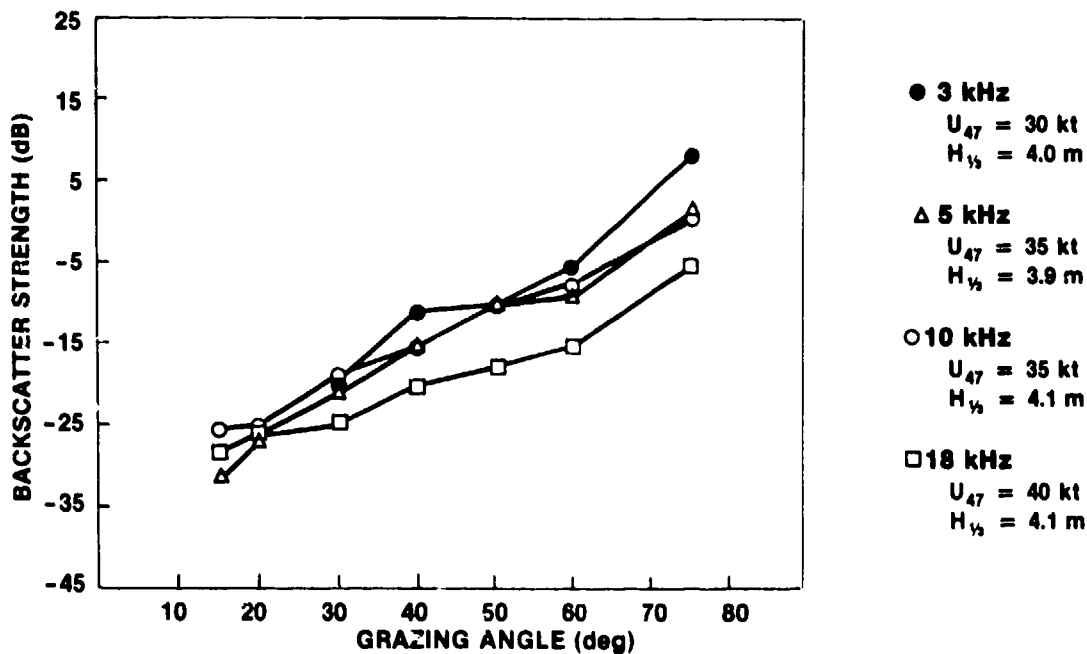


Figure 4-6. Backscattering Strength vs. Grazing Angle
for Different Frequencies

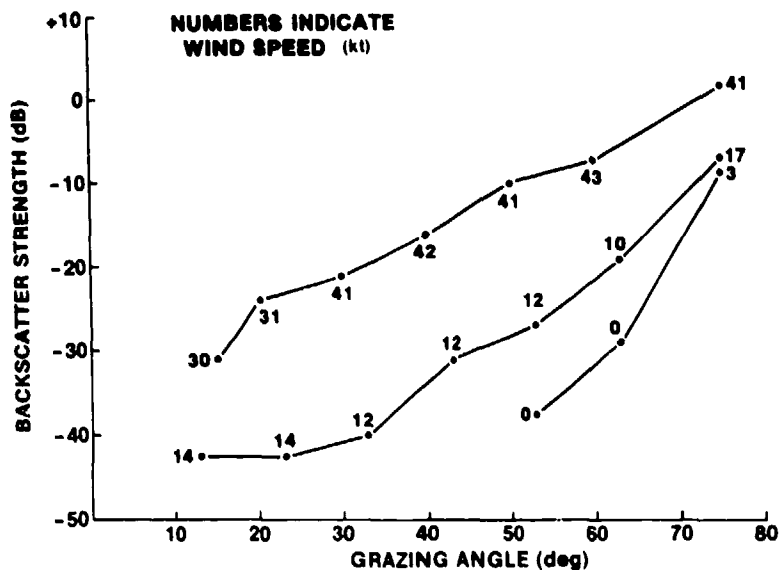


Figure 4-7. Backscattering Strength vs. Grazing Angle at 10 kHz for Different Wind Speeds

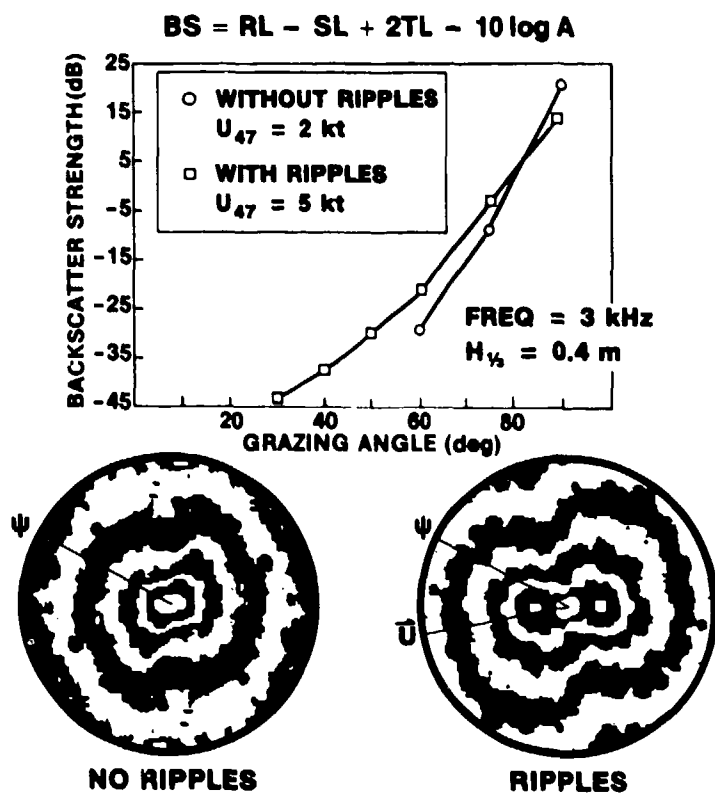


Figure 4-8. Backscattering Strength at 3 kHz With and Without Sea Surface Ripples

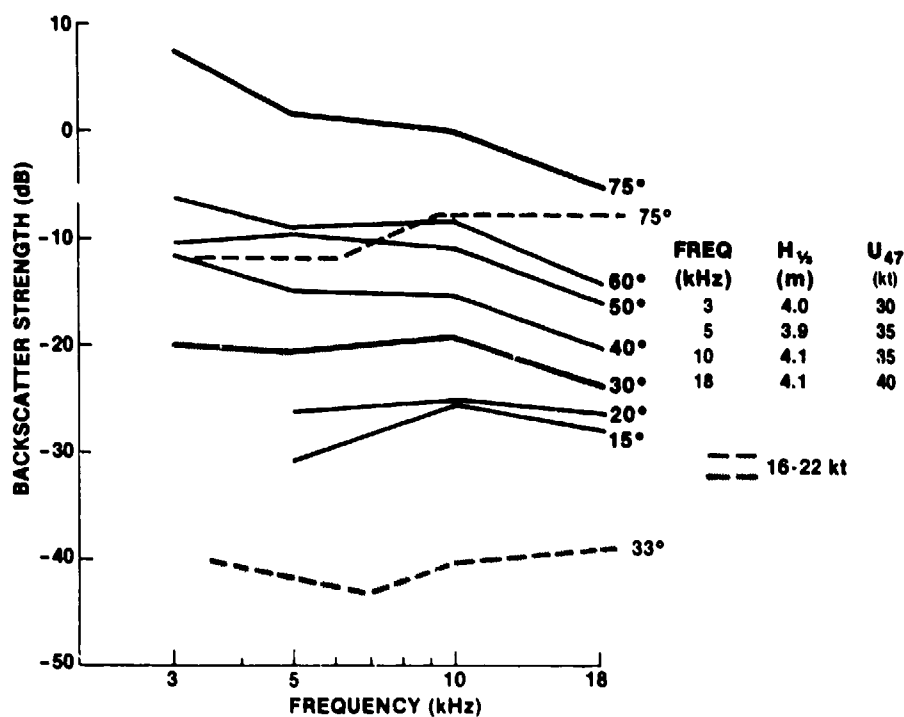


Figure 4-9. Frequency Dependence of Backscatter at Various Grazing Angles

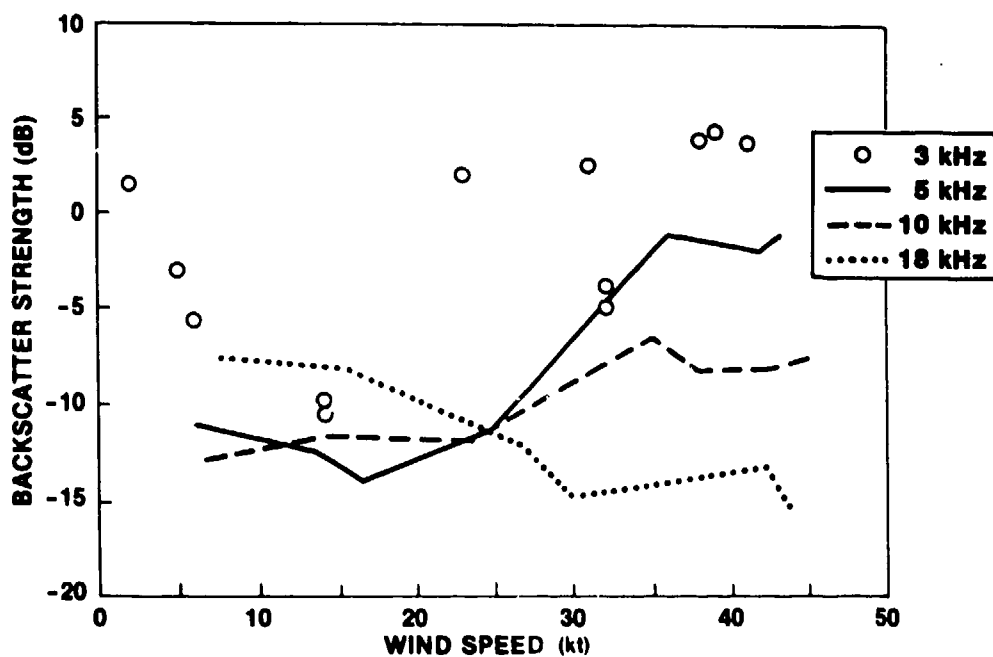


Figure 4-10. Normal Incidence Backscatter vs. Wind Speed

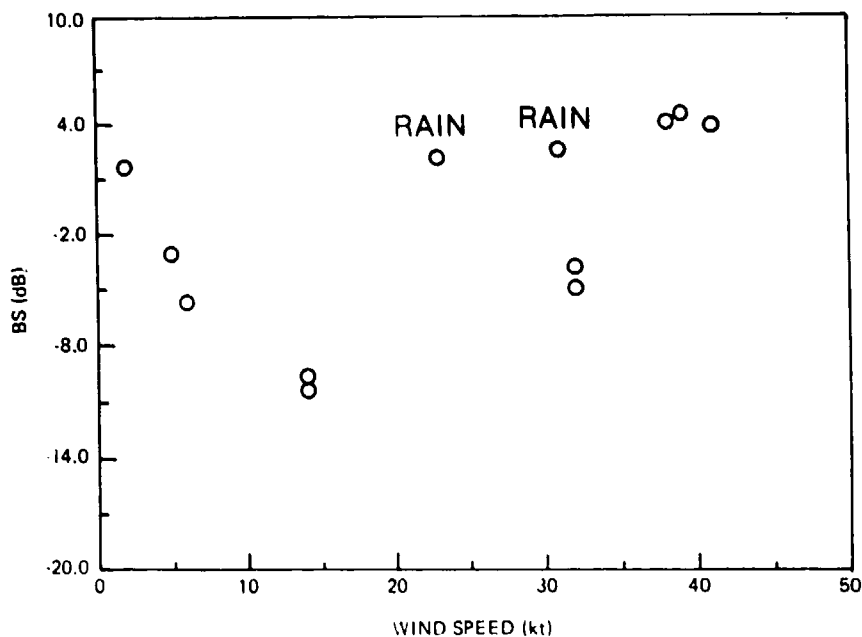


Figure 4-11. Normal Incidence Backscatter Illustrating the Effect of Rainfall

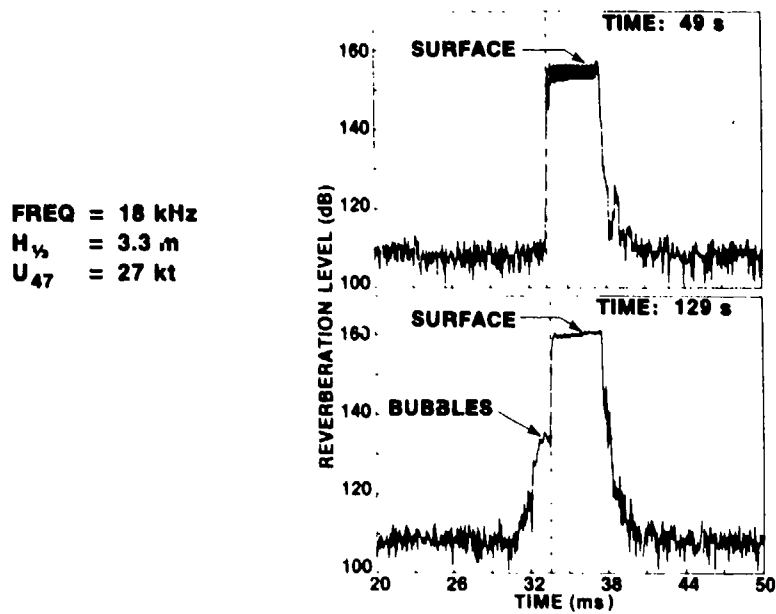


Figure 4-12. Single Ping Acoustic Reverberation at Normal Incidence

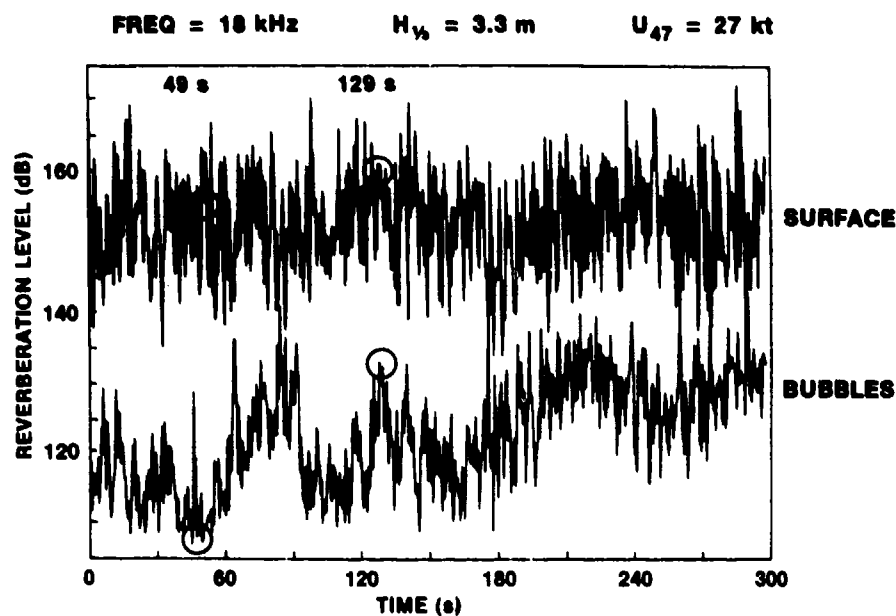


Figure 4-13. Reverberation Level vs. Time From Surface and Bubble Scatterers at Normal Incidence

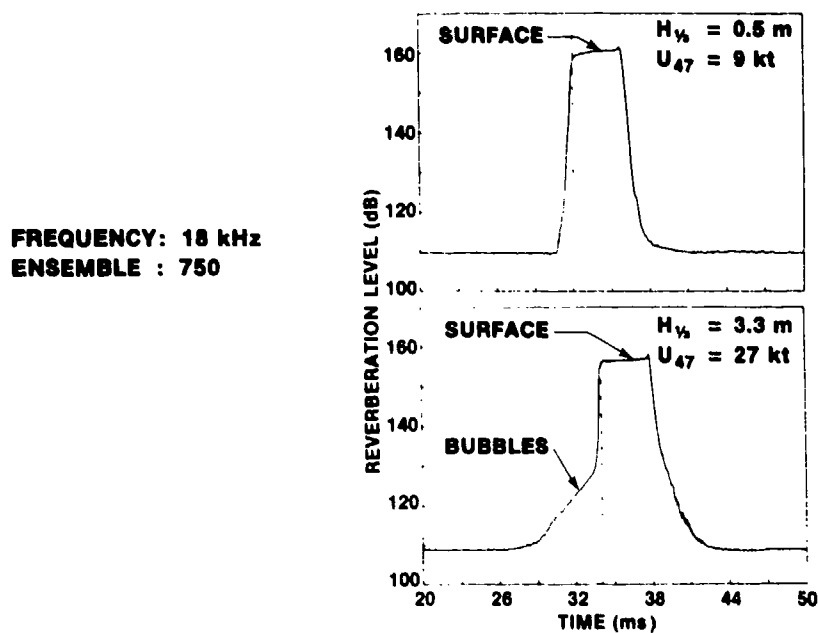


Figure 4-14. Ensemble-Averaged Acoustic Reverberation at Normal Incidence

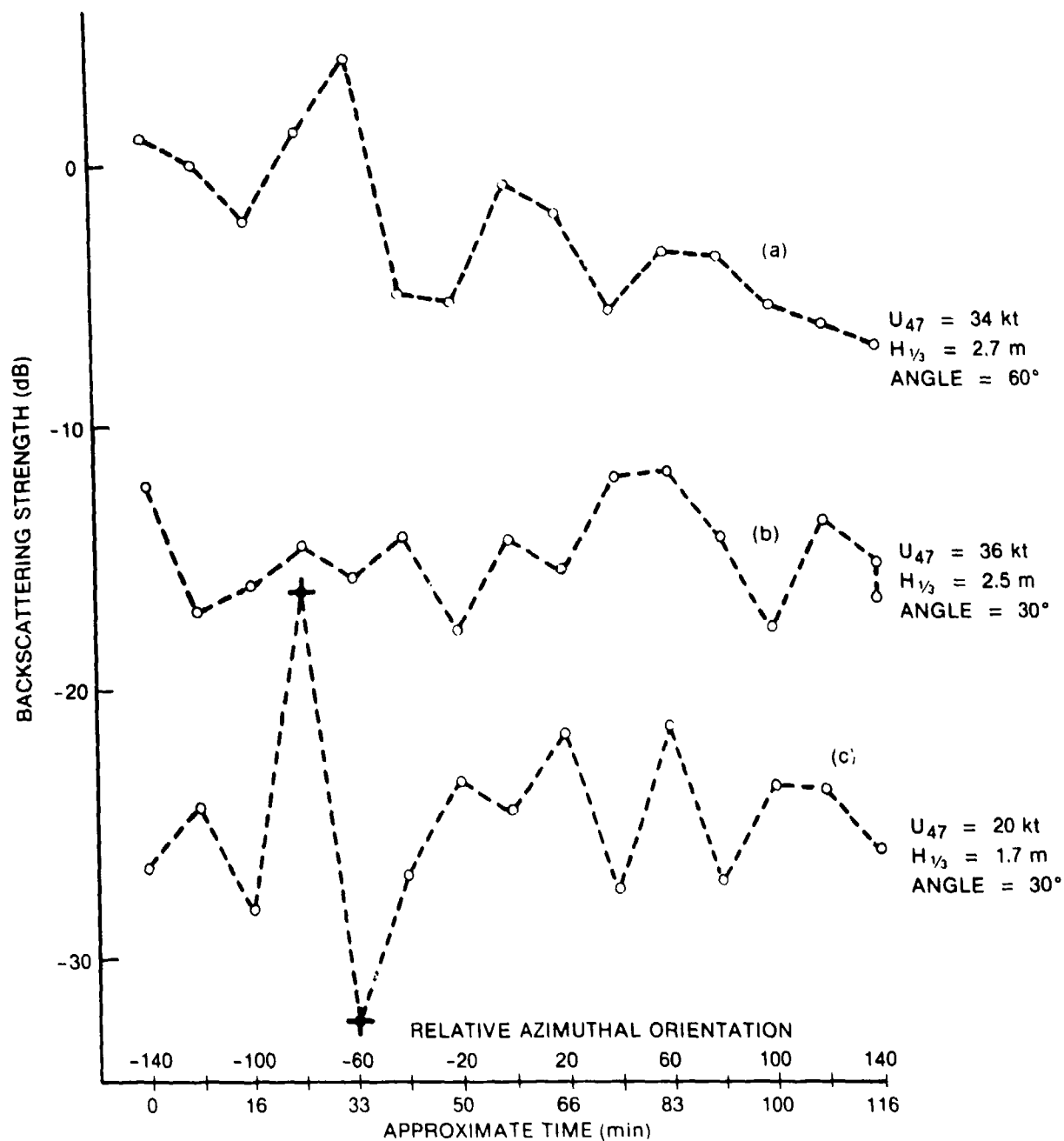


Figure 4-15. Variability of Backscattering Strength at 3 kHz

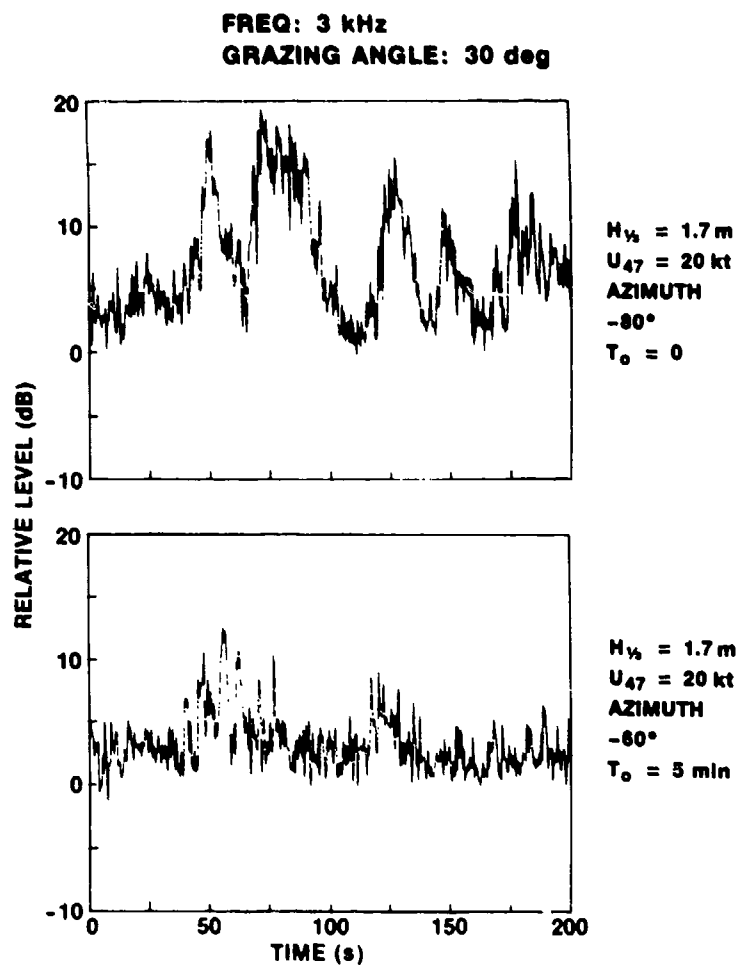


Figure 4-16. Time History of Backscatter Energy

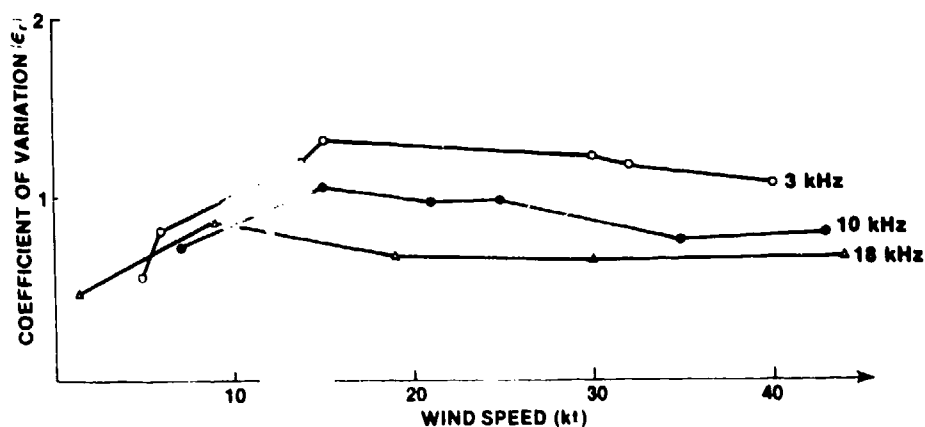


Figure 4-17. Coefficient of Variation for Three Frequencies as a Function of Wind Speed for a 30-deg Grazing Angle

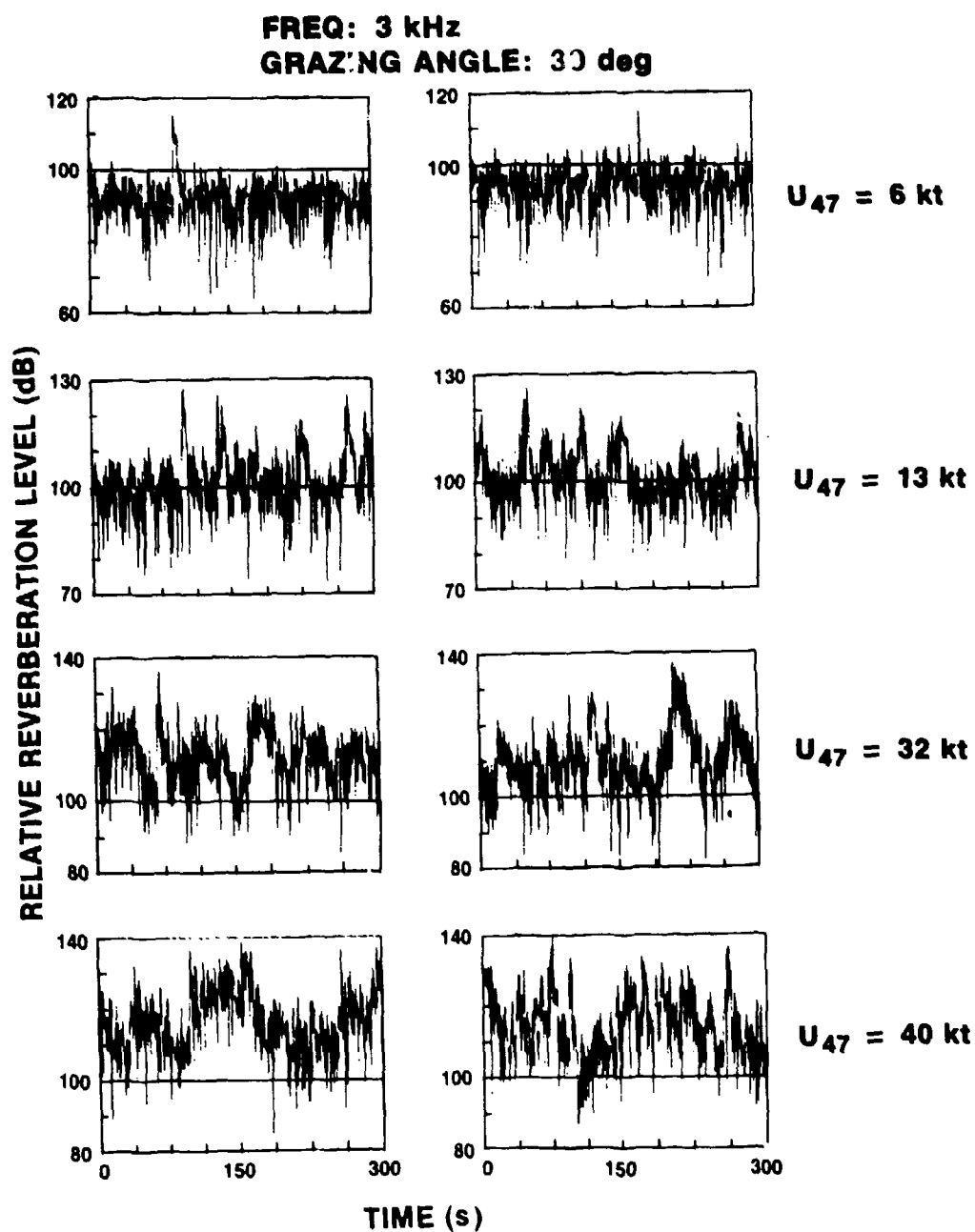


Figure 4-18. Time History of Backscatter Energy
for Different Wind Speeds

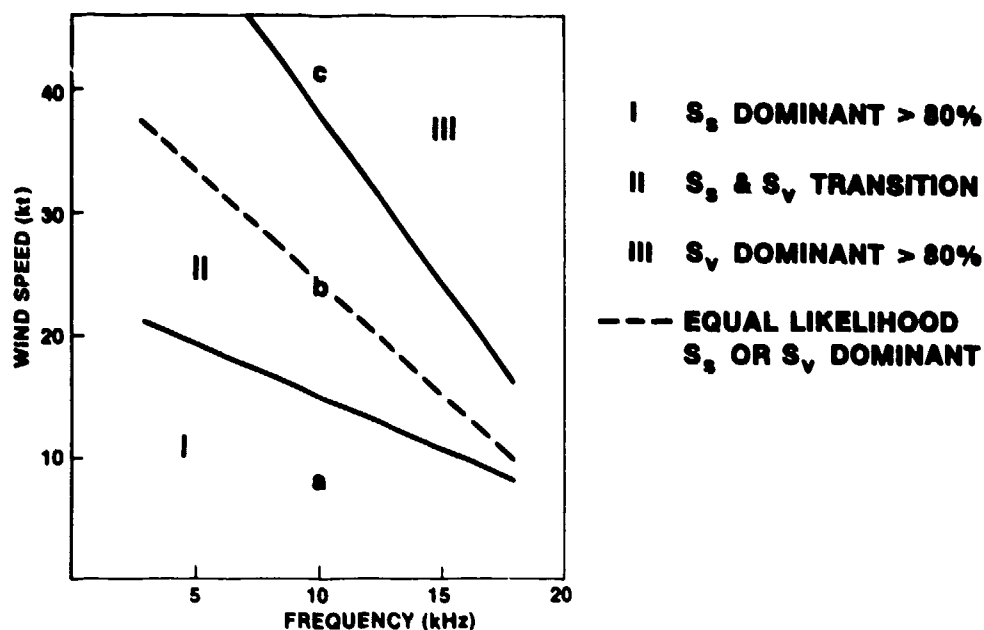


Figure 4-19. Scattering Mechanism Contribution as a Function of Wind Speed and Frequency at a 30-deg Grazing Angle

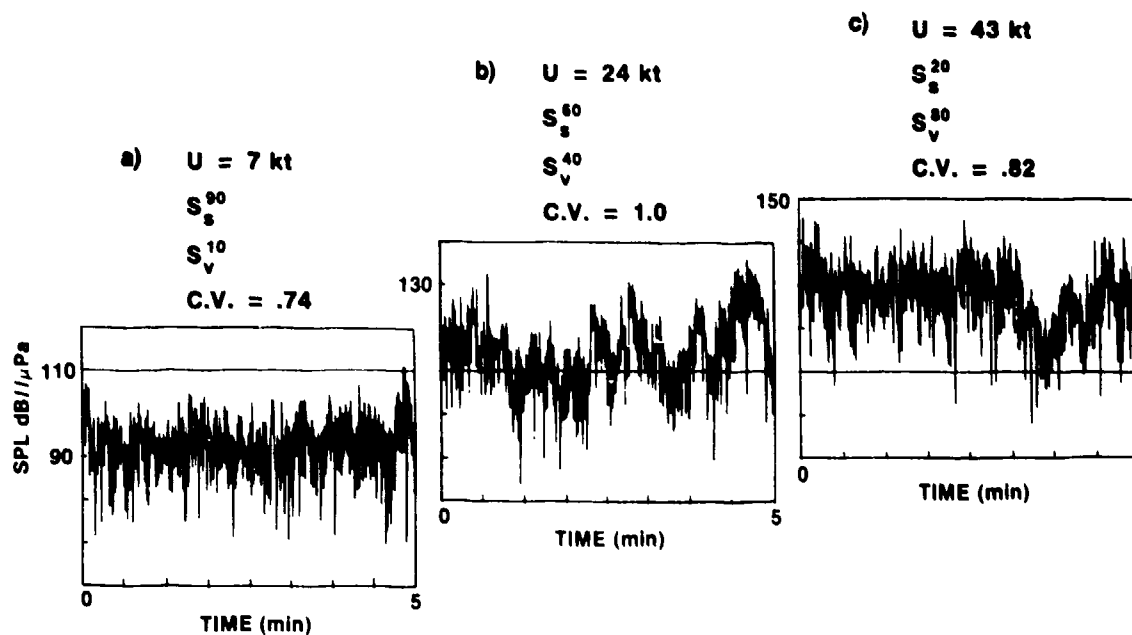


Figure 4-20. Temporal Variability of Backscatter at 10 kHz for a 30-deg Grazing Angle at Three Wind Speeds

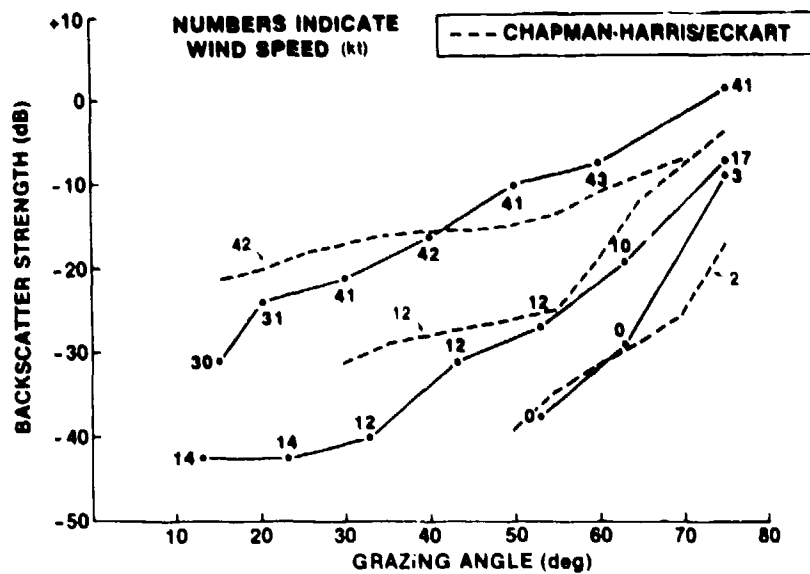


Figure 4-21. Comparison of Chapman-Harris and Eckart Semiempirical Model With NOREX-85 Data

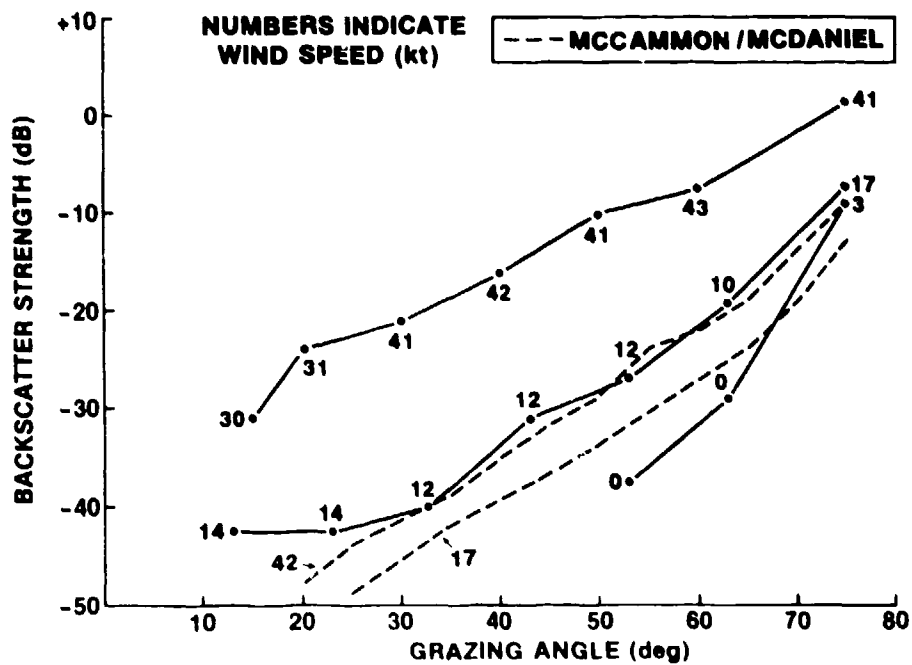


Figure 4-22. Comparison of McCammon and McDaniel Theoretical Model With NOREX-85 Data

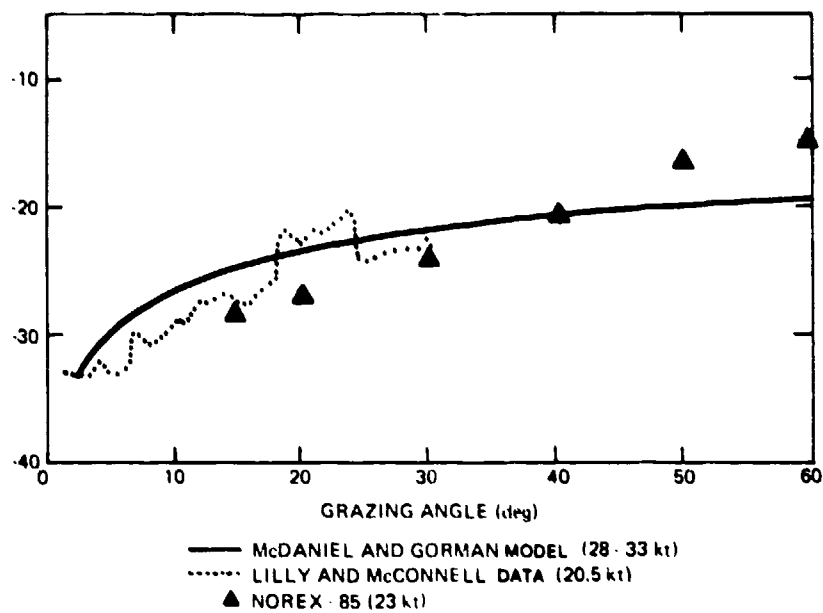


Figure 4-23. Comparison of McDaniel and Gorman Theoretical Model and Measured Data With NOREX-85 Data

5.0 CONCLUSIONS

- There are three regions where different physical processes significantly contribute to acoustic scattering near the sea surface. These areas are dependent on wind speed, frequency, and grazing angle.

Region I (no subsurface bubbles present): The dominant scattering mechanism is closely related to the high frequency wavenumber spectrum of the sea surface. These short wavelengths influence the acoustic backscattering strength at all grazing angles. In this region backscattering is a stationary process except in a transition regime where a glossy sea surface contains high frequency patches that are caused by wind gusts.

Region II (onset of subsurface bubbles): The typical feature in this region is that the time history of backscattering strength shows strong fluctuations in mean level and standard deviation. The scattering is caused by two different mechanisms: (1) high frequency sea surface waves and (2) subsurface bubble populations induced by sea surface wave action and breaking. The increase in backscattering strength, which occurs for short periods of time, can be caused by bubble plumes. The bubbles within these plumes have a large distribution of diameters, and thus the total volume of bubbles present is responsible for the increase in backscattering strength, not bubble resonance only. Backscattering in this region is a non-stationary process.

Region III (high subsurface bubble concentrations): In this region backscattering again approaches a stationary process because, at high wind speeds, sea surface wave action produces a large number of breaking waves. These breaking waves produce high density subsurface bubble populations that acoustically mask the surface. Therefore, the backscattering in this region is due to the total volumetric bubble population and not to the sea surface.

At a 30-degree grazing angle, scattering covers all three regions.

- Acoustic backscattering strength reaches saturation at high wind speeds and at all grazing angles. The scattering mechanism causing saturation at high grazing angles is sea surface roughness; at low grazing angles, the cause is subsurface bubbles. The saturation onset occurs at lower sea states for higher frequencies and lower grazing angles. There is a strong frequency dependence in the saturation region; i.e., as frequency increases, backscattering strength decreases.
- There is a frequency dependence for backscattering at high wind speeds and high grazing angles. This dependence decreases at low grazing angles.

- At normal incidence, acoustic backscattering strength increases when rain is present at 3 kHz.
- Good correlation is seen between sonar and radar backscatter data. Both exhibit increased backscatter strengths as wind speed increases.
- Comparison with a theoretical backscattering model that includes bubbles as a scattering mechanism shows good agreement with experimental data at high wind speeds and low grazing angles.

6.0 RECOMMENDATIONS

The significant influence of bubbles on the temporal variability of acoustic backscatter was not expected prior to the experiment. Thus, when pulse length, pulse repetition rate, number of pings per event, etc., were scheduled before the experiment, it was assumed that all effects caused by ocean waves were covered. The subsequent data analysis showed some surprising results; that is, bubble plumes become an important scattering mechanism even

- at low frequencies,
- at relatively low wind speeds,
- at high grazing angles, and
- at small insonified volumes.

It should again be mentioned that the transmitter has a very small beamwidth, which made it possible to discover bubble effects. Conventional sonars, which have a broader beamwidth and work with longer pulse lengths, would probably not see the effects due to single bubble plumes, and, thus, the time history would not show strong variability even in the intermediate wind speed region. To derive a sufficiently exact statistical estimation of backscattering strength for the intermediate wind speed region, the measuring time for one event should be on the order of 1 to 2 hours. On the other hand, there is a limitation in measuring time because of the relatively rapid change in weather conditions in the area where the data were taken.

Future measurements could be made with a transmitter that has a broader beamwidth. This would increase the amount of bubble plumes measured at the same time and thus would decrease measuring time. Unfortunately, the broad beamwidth could cause multipath problems when the experiment is conducted in shallow water.

Another possibility is the use of the NOREX-85 transmitter. The data analysis could concentrate on the determination of acoustic effects caused by single bubble plumes or by small areas of the sea surface. The analysis would require an exact measurement of the environment. The experiment described in this report showed that the measurement of the directional high frequency ocean wavenumber spectra using Stilwell's technique only yields qualitative information. Short-term effects, like "cat-paws," could only be seen if the photographs were taken at the right spot at the right time. This is only possible for certain geometries of the sun's position and the insonified area of the sea surface that produces the correct amount of light at the insonified spot. Effects like foam on the sea surface further limit use of this technique. Environmental measurements, which do not interfere with the acoustic measurements but give continuous results parallel to the acoustic results, might include electromagnetic backscatter or measures of wind stress. Radar measurements would give information about the slope of the sea surface wave while the wind stress measurement provides information

about the production of solitons or cat paws. When bubbles become the important scattering mechanism, not only the knowledge of the bubble spectrum but information about the larger bubbles in plumes is significant. As long as bubbles are measured optically, there is no obvious means of measuring them in parallel to the acoustic measurements at the same spots without interfering with the acoustics. Future environmental measurements should include the measurement of bubbles, even very large bubbles in plumes close to the surface, to achieve a better understanding of their effects on acoustic scattering phenomena.

7.0 REFERENCES

1. H. Baur, Digital berechnete STILWELLSche Richtungsspektren des Seegangs in Vergleich mit Daten oberflächengebundener Messungen, FWG-Bericht 1980-19, Kiel, Federal Republic of Germany, 1980.
2. S. Gowing and S. C. Ling, "Measurements of Microbubbles in a Water Tunnel," Presented at The 19th American Towing Tank Conference, University of Michigan, Ann Arbor, Michigan, April 1981.
3. M. B. Moffett, "Parametric Arrays," Encyclopedia of Science and Technology, 5th Edition, McGraw-Hill Book Co., Inc., NY, April 1982, pp. 814-816 (Reprinted in Scientific and Engineering Studies in Nonlinear Acoustics, 1954 to 1983, Naval Underwater Systems Center, p. I-1).
4. M. B. Moffett and R. H. Mellen, "Model for Parametric Acoustic Sources," Journal of the Acoustical Society of America, vol. 61, no.2, February 1977, pp. 325-337.
5. B. Nuetzel and R. Jacobsen, Beschreibung des Nachhall-Messplatzes, Interner FWG-Bericht 1985-7, Kiel, Federal Republic of Germany, 1985.
6. J. M. Monti, "The Production and Utilization of a Synthetic Sampling Frequency as Applied to Quadrature Demodulation for Envelope Detection," NUSC Technical Memorandum 841024, Naval Underwater Systems Center, New London, CT, 5 April 1984.
7. O. D. Grace and S. P. Pitt, "Sampling and Interpolation of Bandlimited Signals by Quadrature Methods," Journal of the Acoustical Society of America, vol. 48, no. 6, 1970, pp. 1311-1318.
8. P. D. Koenigs, J. M. Monti, B. Nuetzel and H. Herwig, Acoustic Scattering From the Sea Surface, NUSC Technical Document 7291/FWG-Bericht 1984-14, Naval Underwater Systems Center, New London, CT, 1 November 1984.
9. W. J. Pierson, Jr., and L. Moskowitz, "A Proposed Spectra Form for Fully Developed Wind Seas Based on the Similarity Theory of S. A. Kitaigorodskii," Journal of Geophysical Research, vol. 69, no. 24, December 1964, pp. 5181-5190.
10. D. Stilwell, "Directional Energy Spectra of the Sea from Photographs," Journal of Geophysical Research, vol. 74, 1969, pp. 1974-1986.
11. M. Su, NOREX 85 Bubble and Wave Measurements and Their Applications, NORDA Technical Report (In Preparation).
12. P. D. Koenigs, Transient Response of Multidimensional Arrays, NUSC Technical Report 7193, Naval Underwater Systems Center, New London, CT, 26 June 1984.

REFERENCES (Cont'd)

13. F. G. Bass and I. M. Fuks, Wave Scattering From Statistically Rough Surfaces, Pergamon Press, Inc., NY, 1979.
14. C. S. Clay and H. Medwin, Acoustical Oceanography: Principles and Applications, Wiley Interscience, NY, 1977, p. 234.
15. S. A. Thorpe, "On the Clouds of Bubbles Formed by Breaking Waves in Deep Water and Their Role in Air-Sea Gas Transfer," Philosophical Transactions of the Royal Society of London, A 304, 1982, pp. 155-210.
16. S. A. Thorpe and P. N. Humphries, "Bubbles and Breaking Waves," Nature, vol. 283, no. 5746, 31 January 1980, pp. 463-465.
17. S. A. Thorpe, "Bubbles in a Freshwater Lake," Nature, vol. 279, 31 May 1979, pp. 403-405.
18. R. J. Urick, Sound Propagation in the Sea, Defense Advanced Research Projects Agency, U.S. Government Printing Office, Washington, DC, 1979.
19. G. Garrison, S. Murphy, and D. Potter, "Measurements of the Backscattering of Underwater Sound From the Sea Surface," Journal of the Acoustical Society of America, vol. 32, no. 1, January 1960, pp. 104-111.
20. P. Wille and D. Geyer, "Measurements of Wind-Dependent Acoustic Transmission Loss in Shallow Water Under Breaking Wave Conditions," Presented at The 12th Acoustic Symposium on Underwater Acoustics, Halifax, Canada, 16-18 July 1986.
21. S. McDaniel and D. McCammon, "Composite Roughness Theory Applied to Fetch-Limited Seas," The Pennsylvania State University Technical Memorandum File No. 86-40, Applied Research Laboratory, 21 March 1986.
22. F. Bendat and A. Pierson, Random Data: Analysis and Measurement Procedures, Wiley-Interscience, NY, 1971.
23. D. Middleton and R. Mellen, "Wind-Generated Solitons: A Potentially Significant Mechanism in Ocean Surface Wave Generation and Surface Scattering," IEEE Journal of Oceanic Engineering, vol. OE10, no. 4, October 1985, pp. 471-476.
24. R. Chapman and J. Harris, "Surface Backscattering Strength Measured With Explosive Sound Sources," Journal of the Acoustical Society of America, vol. 34, no. 10, October 1962, pp. 1592-1497.
25. S. McDaniel and A. Gorman, "Acoustic and Radar Sea Surface Scatter," Journal of Geophysical Research, vol. 87, no. C6, 20 May 1982, pp. 4127-4136.

REFERENCES (Cont'd)

26. B. Nuetzel, H. Herwig, J. M. Monti, and P. D. Koenigs, A Further Investigation of Acoustic Scattering From the Sea Surface, NUSC Technical Document 7685/FWG-Bericht, 1986-3, Naval Underwater Systems Center, New London, CT, 9 July 1986.

INITIAL DISTRIBUTION LIST

Addressee	No. of Copies
COMOPTEVFOR	1
COMSURFWARDEVGRU	1
COMSUBDEVGRUONE	1
COMSUBDEVRON 12	1
ASN (RE S)	1
OASN (Spec Dep for Adv Concept)	1
Deputy USDR E (Res Adv Tech)	1
OUSDR E (Res Adv Tech)	2
OCNR (OCNR-11, -122, -1221, -1245, -131, -132, -20, -231, -234, -2411 (R. Farwell))	10
CNO (NOP-951, -952, -098, -981, -983, -03)	6
DIA, DT-2C	1
NRL (E. Franchi, R. Palmer, F. Erskine, W. Keller, R. Pitre, Code 8314)	6
NORDA (Code 113, -240, -241, -243, -245, -260, -270, -330, -331, W. Kinney, M. Su, Library)	12
SPAWAR (PMW-180-5)	1
NAVOCEANO (Code 02, -6200)	2
NAVSEASYS COM (SEA-63, -63D, -63Y)	3
NAVAIRDEV CEN	1
NOSC (J. W. Young, R. Smith, Code 8302, Code 6565 (Library))	4
NAVCOASTSYSCTR	1
NSWC (Code U31)	1
NISC	1
NAVPGSCOL (Library, H. Medwin, S. W. Yoon)	3
NAVWARCOL	1
DTIC	12
DARPA	1
DTNSRDC	1
FWG (G. Ziehm, P. Wille, W. Schmid, H. Baur, H. Herwig (5), B. Nuetzel (5), Bibliothek (36))	50
SACLANTICTR (Tech. Director, J. Marchment, E. Sullivan, R. Martin, Library (2))	6
NOAA/NFC (F. Steimle)	1
Defence Research Establishment Pacific (D. Thomson)	1
Univ. of Miami/RSMAS (H. de Ferrari)	1
Univ. of Rhode Island (L. LeBlanc, M. Wimbush, R. Watts P. Stepanishen)	4
Univ. of Illinois (V. Twersky)	1
APL/UW, Seattle (S. McConnell, E. Thorsos, C. Sienkiewicz)	3
APL/Johns Hopkins (A. W. Pattee, E. Byron, A. Boyles, J. Sweeney)	4
ARL/Penn State, State College (S. McDaniel, D. McCammon)	2
ARL, Univ of Texas (H. Bocheme, K. Vaughan)	2

INITIAL DISTRIBUTION LIST (Cont'd)

Marine Physical Lab, Scripps (F. Fisher)	1
Woods Hole Oceanographic Institute (L. G. Frisk, Library)	2
BBN (J. Heine, P. Cable, G. Shephard, J. Zittel, T. Kooij, J. Hanrahan)	6
PSI Marine Sciences (R. Mellen)	1
EDO Corp. (K. Blumenburg, R. Hampton)	2
Gould, Inc. (A. Pavlak, S. Lemon, W. Werner)	3
Raytheon Corp., Submarine Signal Division (P. Bilazarian, F. Fillipini)	2